Utah State University
DigitalCommons@USU

All Graduate Theses and Dissertations | Graduate Studies

5-2011

Study of Geomagnetic Disturbances and Ring Current Variability During Storm and Quiet Times Using Wavelet Analysis and Ground-Based Magnetic Data from Multiple Stations

Zhonghua Xu
Utah State University

Follow this and additional works at: https://digitalcommons.usu.edu/etd

 Part of the Physics Commons

Recommended Citation

Xu, Zhonghua, "Study of Geomagnetic Disturbances and Ring Current Variability During Storm and Quiet Times Using Wavelet Analysis and Ground-Based Magnetic Data from Multiple Stations" (2011). *All Graduate Theses and Dissertations*. 984.
https://digitalcommons.usu.edu/etd/984

This Dissertation is brought to you for free and open access by the Graduate Studies at DigitalCommons@USU. It has been accepted for inclusion in All Graduate Theses and Dissertations by an authorized administrator of DigitalCommons@USU. For more information, please contact digitalcommons@usu.edu.



STUDY OF GEOMAGNETIC DISTURBANCES AND RING CURRENT VARIABILITY DURING STORM AND QUIET TIMES USING WAVELET ANALYSIS AND GROUND-BASED MAGNETIC DATA FROM MULTIPLE STATIONS

by

Zhonghua Xu

A dissertation submitted in partial fulfillment
of the requirements for the degree

of

DOCTOR OF PHILOSOPHY

in

Physics

Approved:

Dr. Lie Zhu Major Professor	Dr. Jan Sojka Committee Member
Dr. Piotr Kokoszka Committee Member	Dr. Vincent Wickwar Committee Member
Dr. Farrell Edwards Committee Member	Dr. Mark R. McLellan Vice President for Research and Dean of the School of Graduate Studies

UTAH STATE UNIVERSITY
Logan, Utah

2011

Copyright © Zhonghua Xu 2011

All Rights Reserved

ABSTRACT

Study of Geomagnetic Disturbances and Ring Current Variability During Storm and Quiet Times Using Wavelet Analysis and Ground-based Magnetic Data from Multiple Stations

by

Zhonghua Xu, Doctor of Philosophy

Utah State University, 2011

Major Professor: Dr. Lie Zhu
Department: Physics

The magnetosphere-ionosphere contains a number of current systems. These currents vary on a wide range of spatial and temporal scales and physically couple with each other. To study the complicated behaviors of these coupled current systems, the ground-based magnetometer has been a useful tool, but the recorded magnetometer data are always multi-scaled and intermittent due to the nature of these current systems. To distinguish these geomagnetic effects with multiple temporal and frequency scales, the wavelet analysis technique is especially suitable because of its special abilities of presenting information in both temporal and frequency domains. In this dissertation, the geomagnetic disturbances and the ring current variability during storm and quiet times are studied by using wavelet analysis and ground-based magnetic data from multiple stations. The first part of this dissertation investigates the strengths of applying the wavelet procedure to geomagnetic data for ring current study during storm and quiet periods. The second part of this dissertation characterizes the geomagnetic effects caused by symmetric and asymmetric components of ring currents during storm and quiet times by applying wavelet analysis to geomagnetic data from multiple stations. The third part of this dissertation studies the spatial variability of the symmetric ring current by applying the wavelet analysis technique to multiple

components of magnetic data from multiple stations. The results show the unique strengths of the wavelet method allow us to quantitatively distinguish the geomagnetic effects on ring current variations from other M-I current systems. The unique strengths of wavelet method also allow us to separate the magnetic effects of the symmetric ring current from those caused by the asymmetric ring current. Quantitative information of the spatial variability of the ring currents is essential for understanding the dynamics of the ring currents, as well as the magnetic storm processes. The techniques developed in this dissertation have potential values as space weather monitoring tools for satellite controls, power grids, communication systems, oil pipelines, and other high-tech systems that are vulnerable to the negative impacts of disruptive geomagnetic events.

(106 pages)

ACKNOWLEDGMENTS

A great many people have contributed to this dissertation production. I owe my gratitude to all those people who have made this dissertation possible and, because of whom, my graduate experience has been one I will cherish forever.

I would like to thank my advisor, Dr. Lie Zhu, sincerely and deeply for the guidance over the last five years. Dr. Lie Zhu taught me how to question thoughts and express ideas of my own. His patience and support helped me overcome many critical situations and finish this dissertation. I hope one day I will become as good an advisor to my students as Dr. Lie Zhu has been to me.

I would also like to thank my committee members, Dr. Jan Sojka, Dr. Piotr Kokoszka, Dr. Vincent Wickwar, and Dr. Farrell Edwards, for valuable interactions during my program.

At last, I would like to thank my wife and family for years of support and understanding of my choices.

This research was partially supported by NSF grants DMS0413653, ATM-0533543, and NASA grant NNG05GJ48G. I would like to thank the INTERMAGNET and USGS for the magnetometer data used in this research.

Zhonghua Xu

CONTENTS

Page

ABSTRACT iii

ACKNOWLEDGMENTS v

LIST OF TABLES viii

LIST OF FIGURES x

CHAPTER

1. INTRODUCTION 1

2. DATA DESCRIPTION 9

   2.1. Earth's geomagnetism 9
   2.2. Instruments used for the geomagnetic observations 12
   2.3. Geomagnetic observation networks 15

3. RESEARCH APPROACH 18

   3.1. Why wavelet? 18
   3.2. Comparison between wavelet transform and Fourier transform 19
   3.3. Background of wavelet transforms 20

4. AN ASSESSMENT STUDY OF THE WISA INDEX 25

   4.1. Dst index 25
   4.2. WISA index 26
   4.3. Comparisons between the WISA and the Dst indices 27
   4.4. FFT analysis on the WISA and Dst indices 30
   4.5. Flexibility of the WISA on data stretch 33
   4.6. Effects of varying number of stations on the WISA 35
   4.7. Effects of missing data on the WISA 41
   4.8. Discussions and conclusions 44

5. WAVELET CROSS-SPECTRUM ANALYSIS OF THE RING CURRENT USING MAGNETIC RECORDS FROM MULTIPLE LOW-LATITUDE STATIONS 46

   5.1. Introduction of symmetric and asymmetric components of the ring current . 46
   5.2. Data and method 47
   5.3. Results 50
      5.3.1. Quiet periods study (2001.01.05-01.19 and 2001.06.22-07.07) 50
      5.3.2. Storm periods study (2001.03.18-04.03 and 2001.10.15-10.30) 59
   5.4. Conclusion and discussion 65

6. SPATIAL VARIABILITY OF THE RING CURRENT DURING STORM AND QUIET PERIODS 69

6.1. Mathematical scheme for the study of the symmetric ring current 70
6.2. Four simplified configurations 74
6.3. Study of the radius variations of the symmetric ring current 77
6.4. Discussion and future work 81

7. SUMMARY AND DISCUSSION 86

REFERENCES 89

VITA 94

LIST OF TABLES

Table Page

4.1. The four Dst stations. 27

4.2. Statistical comparisons between the WISA index calculated on different data stretches and the Dst index. 35

4.3. The list of stations used for studying the effects of varying numbers of stations on the WISA. 37

4.4. The combinations of stations used for studying the effects of varying numbers of stations on the WISA. 38

4.5. The difference and Root Mean Squared Errors (RMSE) between 10-station WISA and other numbers of station during March-April, 2001, the quiet time, and the storm time in that period. 40

4.6. Missing data effects during quiet time. 42

4.7. Missing data effects during storm time. 43

5.1. The locations of four Dst Stations. 48

5.2. The correlation coefficients in the UT frame for D8 to D13 for the quiet period during 2001.01.05-01.19. 55

5.3. The correlation coefficients in the LT frame (SJG as reference) for D8 to D13 for the quiet period during 2001.01.05-01.19. 56

5.4. The coefficients in the UT frame after the Sq variation is removed from D8 to D10 compared with the original coefficients for the quiet period during 2001.01.05-01.19. 57

5.5. The averages of absolute magnitudes from D8 to D13 from different stations for the quiet period during 2001.01.05-01.19. 58

5.6. The correlation coefficients in the UT frame from D8 to D13 for the quiet period during 2001.06.22-07.07. 59

5.7. The averages of absolute magnitudes from D8 to D13 from different stations for the quiet period during 2001.06.22-07.07. 60

5.8. The coefficients in the UT frame from D8 to D13 for the storm period during 2001.03.18-04.03. 63

5.9. The coefficients in the LT frame from D8 to D13 for the storm period during 2001.03.18-04.03. 64

5.10. The coefficients in the UT frame after the Sq variation removed from D8 to D10 comparing with the original coefficients for the storm period during 2001.03.18-04.03. 64

5.11. The averages of absolute magnitudes from D8 to D13 from different stations for the storm period during 2001.03.18-04.03. 65

5.12. The coefficients in the UT frame from D8 to D13 for the storm period during 2001.10.15-10.30. 66

5.13. The average absolute magnitudes from D8 to D13 from different stations for the storm period during 2001.10.15-10.30. 66

LIST OF FIGURES

Figure Page

1.1. Schematic diagram of various current systems in the magnetosphere-ionosphere. 1

1.2. The field-aligned current system with two shells of magnetic field lines connecting the magnetosphere to the ionosphere. 3

1.3. The variations of Horizontal (H) component of the geomagnetic field at HON station during the storm from Julian day 82 to day 101 in year 2001. 4

2.1. A sketch showing the Earth's magnetic field is similar to the magnetic field generated by a bar magnet. 10

2.2. Simulation of Earth's core by Gary Glatzmaier et al. Los Alamos National Labs. 10

2.3. The seven components of the geomagnetic field vector. 11

2.4. A schematic of the fluxgate magnetometer. 13

2.5. A schematic of the proton precession magnetometer. 15

2.6. The map of INTERMAGNET Magnetic Observatory. 16

2.7. The geographic distribution of the USGS observatories. 17

3.1. Details (D1 to S10) of maximum overlap discrete wavelet transform (MODWT) for one quiet day (2001.01.05). 24

4.1. The WISA index, Dst index, and their differences for the period March-April 2001. 28

4.2. The scatter plot of the WISA and Dst indices for the period of March-April 2001. 29

4.3. The FFT results of the WISA, Dst indices, and their difference for the period of March-April 2001. 31

4.4. The WISA index and the inverse FFT peak components of 24-, 12-, 8-, and 6-hour periods for the period of March-April 2001. 32

4.5. The WISA, Dst indices, and their difference for the Julian days 86-93 in year 2001. 34

4.6. The scatter plot of the WISA and Dst indices for Julian days 86-93 in year 2001. 34

4.7. The 10-station WISA, the Dst and the difference between them for the period of March-April 2001. 39

4.8. Missing data distributions of geomagnetic observatories SJG and HON in year 2001. 43

5.1. The Dst index for the quiet period (a) (2001.01.05-01.19), and the storm period (b) (2001.03.18-04.03). 49

5.2. MODWT Details (D1-D10) and Smooth (S10) for one quiet day (2001.01.05). 51

5.3. MODWT Details (D11 and D12) for the quiet period during 2001.01.05-01.19 (Julian Day 5-19) in the UT frame. 53

5.4. MODWT Details (D8 and D9) for the quiet period during 2001.01.05-01.19 (Julian Day 5-19) in the UT frame. 54

5.5. MODWT Details (D11 and D12) for the storm period during 2001.03.18-04.03 (Julian Day 77-93) in the UT frame. 61

5.6. MODWT Details (D8 and D9) for the storm period during 2001.03.18-04.03 (Julian Day 77-93) in the UT frame. 62

6.1. Artist's rendition of the symmetric ring current over the Earth's magnetic equatorial region. 71

6.2. The dipole field model of Earth's magnetic field by the courtesy of Dr. Daniel I Golden. 71

6.3. The differences between keeping 2nd and 1st order terms in the vector potentials. 75

6.4. The radius variations of the symmetric ring current in 2001 for quiet (upper figure) and storm (lower figure) periods. 79

6.5. The radius variations of the symmetric ring current in 2002 for quiet (upper figure) and storm (lower figure) periods. 81

CHAPTER 1

INTRODUCTION

The magnetosphere-ionosphere system contains a number of current systems, such as the magnetopause current, the ring current, the cross-tail current, the field-aligned current, and various electrojets in the ionosphere. These currents vary on a wide range of spatial and temporal scales and are physically coupled with each other. As shown in Figure 1.1 [1], different current systems generate effects in different regions on the Earth.

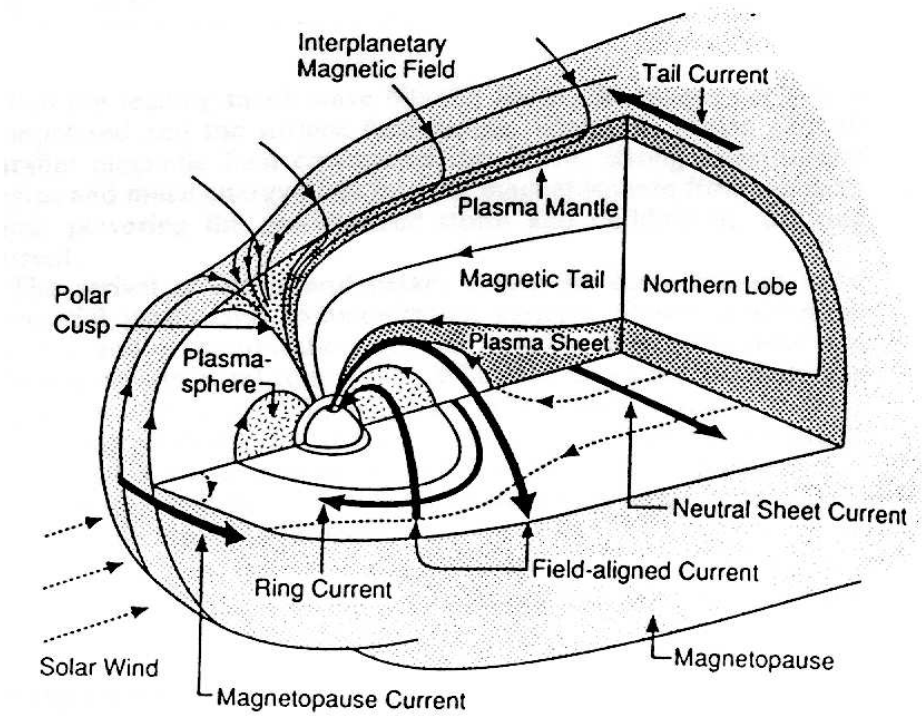


Fig. 1.1. Schematic diagram of various current systems in the magnetosphere-ionosphere.

The magnetopause current flows over the outside surface of the magnetosphere. The distance is about 7-10 Re (the radius of the Earth). The magnetic field associated with the magnetopause current is observable at the surface of the Earth. This is particularly true during times when the magnetopause is compressed Earthwards, leading to an increase in

the magnetic field measurable at the Earth's surface. This effect leads to an increase of the value of the geomagnetic activity index at the start of a geomagnetic storm, while the subsequent intensification of the ring current leads to major decrease of the magnetic field on the Earth's surface.

The ring current drifts azimuthally around the Earth at radial distances of about 2-7 Re (Earth radii), overlapping the radiation belt region. It consists of trapped 10 - 200 keV ions (mainly H+, He+, and O+) and electrons. The drift is a combined curvature and gradient drift, which is eastward for electrons and westward for ions, i.e., the direction of the current is westward. The strength of the ring current can be monitored by ground-based magnetometers at middle or equatorial latitudes since the ring current will cause negative disturbances of the magnetic field on the Earth's surface.

The field-aligned currents appear as closed current loops within the magnetosphere and the ionosphere as a consequence of the tangential drag of the magnetosphere on the solar wind. The field-aligned currents flow on two shells completely surrounding the Earth. As shown in Figure 1.2, the higher latitude shell is usually referred to as Region 1 current and the lower one as Region 2 current [2].

There are other currents, such as the electrojets, in the magnetosphere-ionosphere system. There are three electrojets, the equatorial electrojet that is in the E region above the magnetic equator, and the westward electrojet and eastward electrojet (auroral electrojets) that are in the auroral regions. The electrojets are mainly the Hall currents carried primarily by electrons at altitudes from 100 to 150 km. The electrojets have significant effects on geomagnetic field variations in low-latitude (the equatorial electrojet) and high-latitude (the auroral electrojets) regions. The temporal and spatial variations of the currents in the M-I system cause geomagnetic disturbances on the Earth. The most significant geomagnetic disturbances occur during geomagnetic storms, which is an important subject with a long history for space physics research. The geomagnetic storm is defined as an interval of time when a sufficiently intense and long-lasting interplanetary convection electric field leads, through a substantial energization in the magnetosphere-ionosphere system, to an intensified

ring current strong enough to exceed some key threshold of the quantifying storm time Dst index [3].

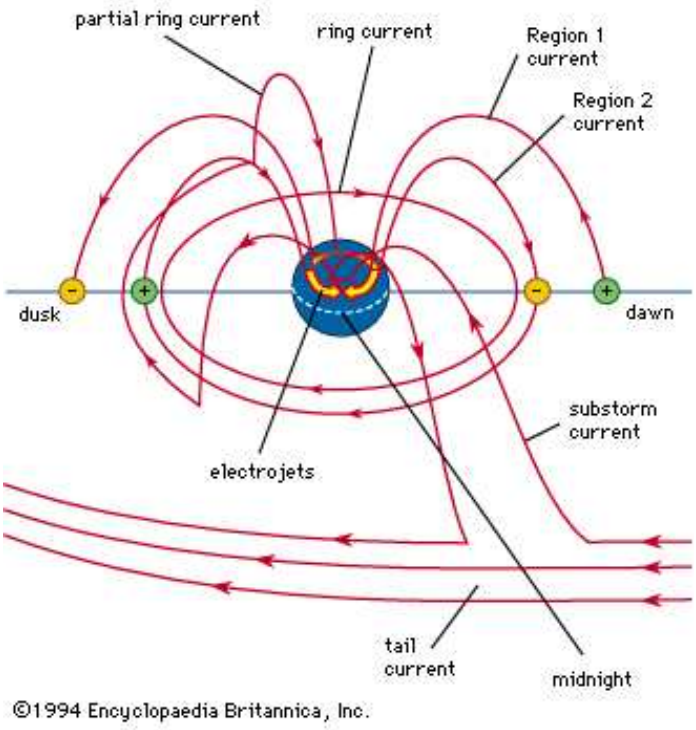


Fig. 1.2. The field-aligned current system with two shells of magnetic field lines connecting the magnetosphere to the ionosphere.

There are usually three phases in a geomagnetic storm: initial phase, main phase, and recovery phase. These three phases can last for from several hours to a few days. Geomagnetic storms are separated into different categories in terms of the magnitude of a geomagnetic disturbances at low-latitude regions, including intense storm of which the disturbance is less than -100nT, moderate storm of which the disturbance is between -100nT and -50nT, and weak storm of which the disturbance is between -50nT and -30nT. The following figure (Figure 1.3) shows an example of geomagnetic storm recorded at the Honolulu Observatory in 2001. The initial phase started on Day 89 (Julian Day). The main phase was late in Day 89 and early in Day 90. The recover phase lasted for a few days

after the main phase. The H (horizontal) component of geomagnetic field decreased over 400 nT during main phase of this strong storm. The widely used storm index, Dst index, is produced by using the geomagnetic records from four low-latitude stations. The detailed information of the Dst will be discussed in later chapters.

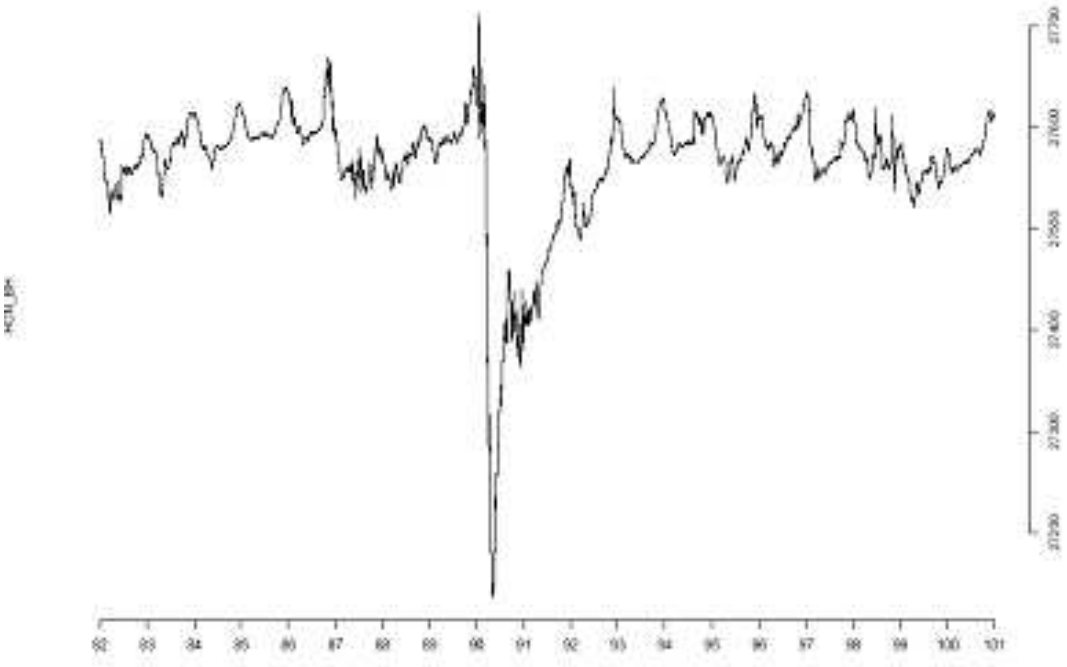


Fig. 1.3. The variations of Horizontal (H) component of the geomagnetic field at HON station during the storm from Julian day 82 to day 101 in year 2001.

The study of geomagnetic storms is an important subject in space physics for understanding the complicated current systems in magnetosphere and ionosphere. During a geomagnetic storm, electric currents, which flow in various regions of the magnetosphere-ionosphere, produce disturbances to the Earth's magnetic fields. The geomagnetic observations record the disturbance effects associated with these current systems. Different current systems generate the effects in different regions on the Earth. For example, the cross-tail current has impacts mainly at the high latitudes since it connects to the field-aligned currents. The ring current has its magnetic effect mainly in the equatorial region. When the ring current is enhanced during storm times, there are negative disturbances of geomagnetic

field at the low latitudes. By studying the geomagnetic effects, the characteristics of these current systems can be revealed.

To characterize the current systems, indices are developed by using geomagnetic records, including Dst, Kp, AE, ASY-H, and SYM-H indices. The AE (Auroral Electrojets) indices, including AE, AU, AL, and AO indices, are produced by the H component from 10-13 observatories along the auroral zone in the northern hemisphere and measure global electrojet activities in the auroral zone. The Kp index is obtained as the mean value of the disturbance levels in the two horizontal field components, observed at 13 selected, subauroral stations. The Kp index is for monitoring global geomagnetic disturbances. The longitudinally asymmetric (ASY) and symmetric (SYM) disturbance indices are introduced to describe the geomagnetic disturbance fields in mid latitudes with high time (i.e., 1 minute) resolution. They are derived for both the H and D components, that is, for the components in the horizontal (dipole pole) direction H (SYM-H, ASY-H) and in the orthogonal (East-West) direction D (SYM-D, ASY-D).

The Dst index is a geomagnetic index that monitors the worldwide magnetic storm level. It is also the standard measure of the ring current activity. It is derived by using the geomagnetic data from four equatorial stations and holds hourly value. The idea of the Dst index was initially created by Kertz [4], [5], and Sugiura [6], and a derivation scheme was proposed later [7]. The International Association for Geomagnetism and Aeronomy (IAGA) version for the Dst was developed by Sugiura [8]. The detailed procedure of the Dst index will be introduced in a later chapter.

The studies on geomagnetic disturbance and the variations of the ring current have been pursued for many years. The classic review of the relation between the ring current and geomagnetic disturbance was performed by Akasofu [9]. The understanding of magnetic storms and substorms was summarized by Kamide et al. [10]. Gonzalez presented a detailed review work of "what is a geomagnetic storm" [3]. The geomagnetic storm effects of H component at low latitudes were studied by Rastogi [11]. The characteristics and causes of intense magnetic storms were addressed by Daglis et al. [12]. Okeke and Hamano studied

the variability of horizontal component of geomagnetic component H with mean quiet-day variation [13]. The statistical modeling of storm level Kp occurrences was introduced by Remick and Love [14].

The research on the ring current is also an important task for space physics scientists. The issues of the ring current dynamics was reviewed by Daglis et al. [12], including the role of substorms in the ring current buildup, the large-scale morphology of the ring current, the mechanism of the ring current decay, and the fidelity of geomagnetic indices that are widely used in storm and ring current studies [15]. The strength of the ring current was studied by Russell and Huddleston [16], Ganushkina et al. [17], Soraas et al. [18], and others. The characteristics of symmetric and asymmetric ring currents during storm phase were studied by Gonzalez et al. [19], Weygand and McPherron [20]. The morphology of the ring current was studied by Le et al. [21] with in-situ magnetic field measurements. The development of the ring current during the great geomagnetic storm of February 1986 was studied by Hamilton et al. [22].

The issue of the efficiency for the ring current index, Dst index, was discussed by Campbell [23] and Karinen and Mursula [24]. The correction or improvement of the Dst index was studied by Karinen and Mursula [25], Wanliss and Showalter [26], and others. The seasonal and diurnal variations of Dst dynamics were investigated by O'Brien and McPherron [27].

Recently, new analysis techniques were applied to geomagnetic data, including wavelet analysis [28], [29], [30], [31], [32], [33], [34], [35], [36], method of natural orthogonal component [37], and lognormal distributions [38].

In this dissertation, the geomagnetic disturbance and the ring current variability are studied by using wavelet analysis and ground-based magnetic data from multiple stations.

First, with a systematic assessment study, the advantages of the wavelet analysis are shown to provide an effective way to separate the geomagnetic effects driven by different currents in the magnetosphere and ionosphere system. The wavelet method is a perfectly suitable tool for studying the time varying data, such as geomagnetic data, because the

wavelet analysis technique has the ability to present information in temporal and frequency domains at the same time. Such ability can be used to separate a time varying signal into time series related with different frequency variations. Applying the wavelet analysis to geomagnetic data can separate the geomagnetic effects connected to different currents in terms of the different frequencies of their variations.

After the geomagnetic variations connected to the ring current variations are extracted by applying the wavelet analysis, the characteristics of these variations are studied in terms of the global symmetric and asymmetric properties for various conditions. The global symmetric variation should have higher correlation between the data from multiple stations than the asymmetric variation. The comparison between the characteristics of the symmetric and asymmetric variations holds valuable information for storm and quiet conditions. Then, the symmetric variations in the geomagnetic data, which come from the global symmetric part of the ring current, are reconstructed to study the spatial and temporal variations of the symmetric ring current. By using sets of physical critera, the variations of the symmetric ring current are categorized into different situations, and different schemes are developed to calculate the temporal and spatial variations of the symmetric ring current from the reconstructed geomagnetic data.

In Chapter 2, the information of the geomagnetic data used in this research is introduced in detail, including geomagnetic field models, magnetometers, observation networks, and data resolutions. In Chapter 3, the wavelet analysis method is presented, including the specific wavelet method, cross spectrum analysis, and comparison with Fourier transforms. In Chapter 4, the strengths of applying the wavelet procedure to geomagnetic data for ring current study is investigated via a quantitative study of the comparison between a wavelet-based storm index and the Dst index. In Chapter 5, the wavelet analysis is used to study the characteristics of the symmetric and asymmetric ring currents with geomagnetic data from multiple stations. In Chapter 6, the variability of the symmetric ring current is studied by applying the wavelet analysis technique to multiple components of magnetic data from multiple stations. Finally, the summary and discussion of this dissertation research

are presented in Chapter 7.

The study of geomagnetic storms has great value for space weather research. The scientific results on the spatial and temporal variability of the ring currents are essential for understanding the dynamics of the ring currents, as well as the magnetic storm processes. The techniques developed in this dissertation research can be very useful for real-time monitoring of the dynamical variations of magnetic storm activities and the spatial and temporal variations of the ring currents. It can be potentially used as a space weather monitoring tool for satellite controls, power grids, communication systems, and oil pipelines, as well as other high-tech systems that are vulnerable to the negative impacts of disruptive geomagnetic events.

CHAPTER 2
DATA DESCRIPTION

2.1. Earth's geomagnetism

In order to describe the geomagnetic storms, the geomagnetic field model needs to be introduced first. The simplest model of the geomagnetic field is similar to the magnetic field generated by a straight magnet. The North Pole of the magnet is close to the magnetic South Pole. The magnetic South Pole of the Earth is close to the geographic North Pole. So the geomagnetic field line on the Earth's surface is going from south to north.

Figure 2.1 shows a sketch of Earth's magnetic field. It shows that Earth's interior has a magnet with its South Pole under Earth's magnetic North Pole. Earth's magnetic field is generated due to a dynamo, which creates large currents in its outer liquid iron core. The dipole axis of the magnetic pole is offset from the axis of the Earth's rotation by about 11 degrees for a geocentric model, which assumes that the center of geomagnetic field is at the same location of the Earth. As a matter of fact, the geomagnetic field is more complicated. First, the center of the field is not at the Earth's center. Second, the offset of the dipole axis is different in north and south regions. The more accurate description is about 11 degrees to the North Pole and 17 degrees to the South Pole due to the location's difference between the rotation center of the Earth and the dipole field center of the geomagnetic field. The following figure (Figure 2.2) shows a simulation of a geomagnetic field generated by the Earth's core.

The geomagnetic field vector (B) has seven components shown in Figure 2.3. The seven components are total intensity (F), declination (D), inclination (I), horizontal component (H), vertical component (Z), north (X) and east (Y) components of the horizontal intensity. For a given location on the surface of the Earth, the magnetic field is given by HDZF or XYZF format, sometimes HDIF format.

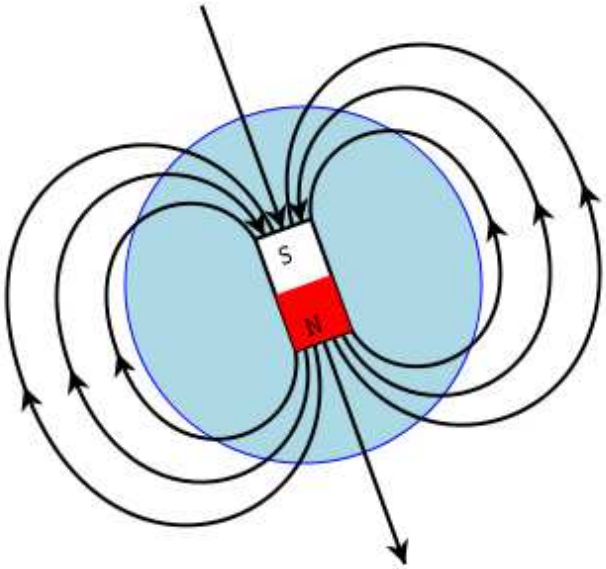


Fig. 2.1. A sketch showing the Earth's magnetic field is similar to the magnetic field generated by a bar magnet.

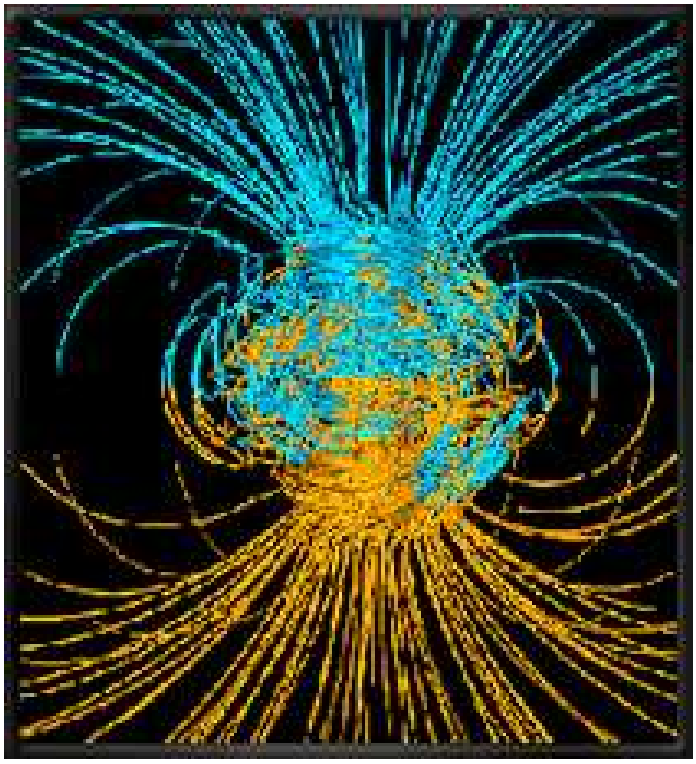


Fig. 2.2. Simulation of Earth's core by Gary Glatzmaier et al. Los Alamos National Labs.

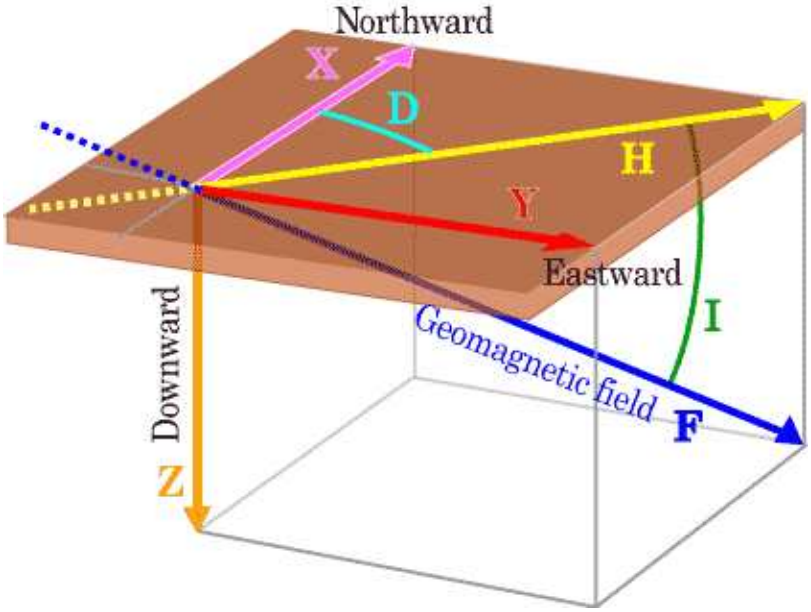


Fig. 2.3. The seven components of the geomagnetic field vector. (Downloaded from http://wdc.kugi.kyoto-u.ac.jp.)

The components can be mutually converted between different formats by using the formulas below:

$$D = arctan\frac{Y}{X} \ . \tag{2.1}$$

$$I = arctan\frac{Z}{H} \ . \tag{2.2}$$

$$F = \sqrt{H^2 + Z^2} \ . \tag{2.3}$$

$$H = \sqrt{X^2 + Y^2} \ . \tag{2.4}$$

The International System of Units (SI) of magnetic field intensity, strictly flux density, most commonly used in geomagnetism is the Tesla. At the Earth's surface, the total inten-

sity varies from 24,000 nanotesla (nT) to 66,000 nT. Other units likely to be encountered are the Gauss (1 Gauss = 100,000 nT) and the gamma (1 gamma = 1 nT).

To describe such a complicated geomagnetic field, several models other than the dipole fields have been developed. One of the most useful models is the International Geomagnetic Reference Field (IGRF). The IGRF uses spherical harmonic coefficients and Geocentric coordinates to represent the scalar potential of the geomagnetic field. The IGRF model provides the seven components according to the variables of longitude, latitude, and altitude on the surface of the Earth. It is released by the International Association of Geomagnetism and Aeronomy (IAGA). The newest version of the IGRF model is 10th generation in 2010. The coefficients for this degree and order 13 main field model were finalized by a task of IAGA in December 2004. The IGRF is the product of a collaborative effort between magnetic field modelers and the institutes involved in collecting and disseminating magnetic field data from satellites and from observatories and surveys around the world. A geomagnetic observatory is a location where absolute and vector measurements of the Earth's magnetic field are recorded accurately and continuously, with a time resolution of one minute or less, over a long period of time. The site of the observatory must be magnetically clean and remain so for the foreseeable future. The earliest magnetic observatories where continuous vector observations were made began operation in the 1840s.

2.2. Instruments used for the geomagnetic observations

There are two main categories of instruments at an observatory. The first category comprises variometers, which make continuous measurements of elements of the geomagnetic field vector, but in arbitrary units, for example, millimeters of photographic paper in the case of photographic systems, or electrical voltage in the case of fluxgates. A fluxgate sensor comprises a core of easily saturable material with high permeability. Around the core there are two windings: an excitation coil and a pick-up coil. If an alternating current is fed into the excitation coil so that saturation occurs and if there is a component of the external magnetic field along the fluxgate element, the pick-up coil outputs a signal not only with the excitation frequency, but also other harmonics related to the intensity of the external

field component. Both analogue and digital variometers require temperature-controlled environments and installation on extremely stable platforms (though some modern systems are suspended and therefore compensate for platform tilt). Even with these precautions they can still be subject to drift. They operate with minimal manual intervention and the resulting data are not absolute. A schematic of the fluxgate magnetometer is shown below in Figure 2.4.

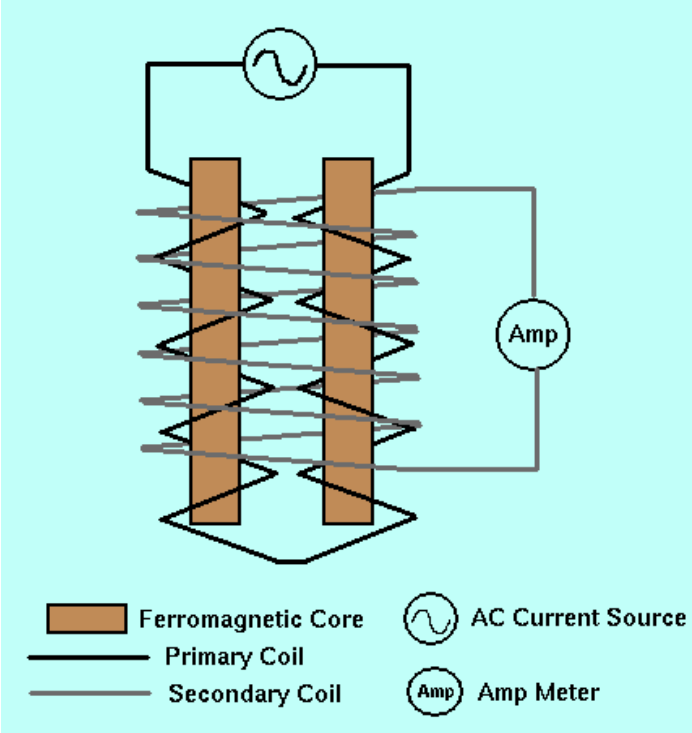


Fig. 2.4. A schematic of the fluxgate magnetometer. (Downloaded from http://www.earthsci.unimelb.edu.au.)

The second category comprises absolute instruments, which can make measurements of the magnetic field in terms of absolute physical basic units or universal physical constants. The most common types of absolute instrument are the fluxgate theodolite for measuring D and I and the proton precession magnetometer for measuring F. In the former, the basic unit is an angle. The fluxgate sensor mounted on the telescope of a nonmagnetic theodolite is used to detect when it is perpendicular to the magnetic field vector. Collimation errors between the fluxgate sensor and the optical axis of the theodolite and within the theodolite

are minimized by taking readings from four telescope positions. With the fluxgate sensor operating in null-field mode, the stability and sensitivity of the sensor and its electronics are maximized. True north is determined by reference to a fixed mark of known azimuth. This can be determined astronomically or by using a gyro attachment. The proton precession magnetometer uses the principle of Earth's field nuclear magnetic resonance to measure very small variations in the Earth's magnetic field. The sensor component of the proton precession magnetometer is a cylindrical container filled with a liquid rich in hydrogen atoms surrounded by a coil. The sensor is connected by a cable to a small unit in which a power supply, an electronic switch, an amplifier, and a frequency counter are housed. When the switch is closed, a DC current delivered by a battery is directed through the coil, producing a relatively strong magnetic field in the fluid-filled cylinder. The hydrogen nuclei, which behave like minute spinning dipole magnets, become aligned along the direction of the applied field. Power is then cut to the coil by opening the switch. Because the Earth's magnetic field generates a torque on the aligned, spinning hydrogen nuclei, they begin to precess around the direction of the Earth's total field. This precession produces a time-varying magnetic field, which induces a small alternating current in the coil. The frequency of the AC current is equal to the frequency of precession of the nuclei. Because the frequency of precession is proportional to the strength of the total field and because the constant of proportionality is known, the total field strength can be determined quite accurately. Measurements with a fluxgate theodolite can only be made manually while a proton magnetometer can operate automatically. A schematic of the proton precession magnetometer is shown below in Figure 2.5.

Besides the fluxgate magnetometer and the proton precession magnetometer, a dip needle is the simplest magnetometer for measuring the inclination of the magnetic field. A torsion balance magnetometer consists of a strong sensor magnet rigidly attached to a mirror and suspended by a strong fiber, which constrains its motion to a single degree freedom of rotation about the long axis of the fiber. A highly conductive piece of nonferrous metal immersed in the field of the sensor conveniently provides a damping force.

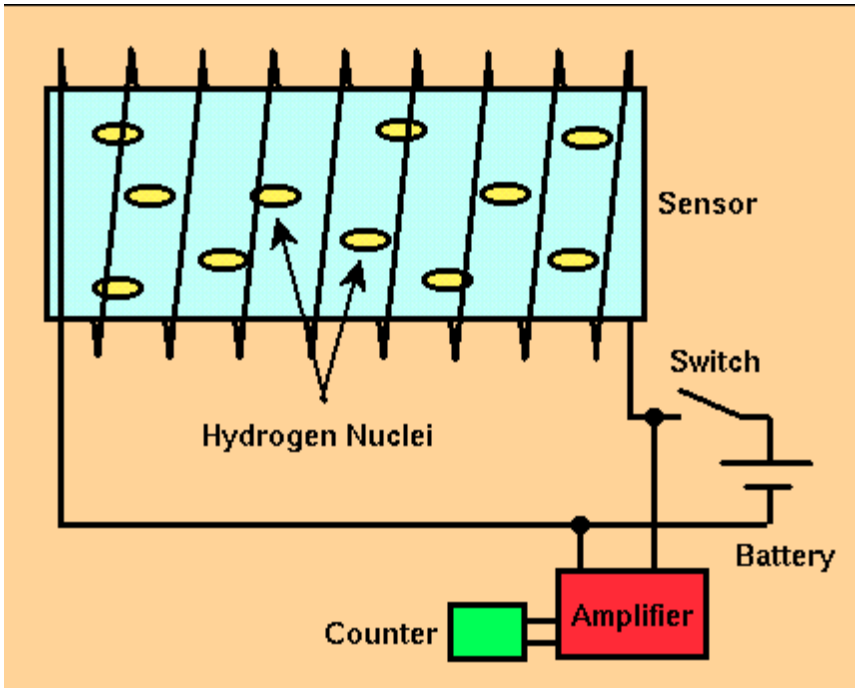


Fig. 2.5. A schematic of the proton precession magnetometer. (Downloaded from http://www. earthsci.unimelb.edu.au.)

2.3. Geomagnetic observation networks

There are hundreds of geomagnetic observatories operating all over the world now. The spatial distribution of the observatories is rather uneven, with a concentration in Europe and a dearth elsewhere in the world, particularly in the ocean areas. The observatories are united into observation networks. One of the largest networks is the INTERMAGNET: International Real-time Magnetic Observatory Network. The INTERMAGNET program exists to establish a global network of cooperating digital magnetic observatories, adopting modern standard specifications for measuring and recording equipment, in order to facilitate data exchanges and the production of geomagnetic products in close to real time. INTERMAGNET has its roots in discussions held at the Workshop on Magnetic Observatory Instruments in Ottawa, Canada, in August 1986 and at the Nordic Comparison Meeting in Chambon La Foret, France, in May 1987. A pilot scheme between the United States and British Geological Surveys was described in the sessions of Division V of the International

Association of Geomagnetism and Aeronomy at the XIXth General Assembly of the International Union of Geodesy and Geophysics in Vancouver, Canada, in August 1987. This scheme used the GOES East satellite to successfully transfer geomagnetic data between the two organizations. INTERMAGNET was founded soon after in order to extend the network of observatories communicating in this way. In order to direct the work and oversee the operations of INTERMAGNET, an Executive Council and an Operations Committee were set up. The first Geomagnetic Information Node (GIN) was established in 1991, and the first CD-ROM/DVD (1991 definitive data) was published in 1993. The observatory in the INTERMAGNET is called the INTERMAGNET Magnetic Observatory (IMO), which provides one minute magnetic field values measured by a vector magnetometer, and an optional scalar magnetometer, all with a resolution of 0.1 nT. Vector measurements performed by a magnetometer must include the best available baseline reference measurement. There are over one hundred IMOs around the world. The map of IMOs is shown in Figure 2.6.

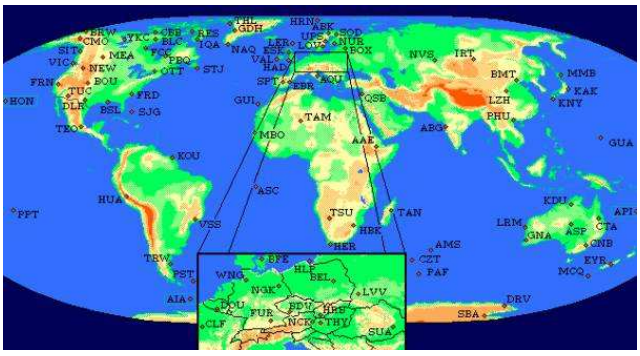


Fig. 2.6. The map of INTERMAGNET Magnetic Observatory. (Downloaded from www .intermagnet. org.)

Another magnetic observatory network is the US Geological Survey (USGS). USGS is a geomagnetic observation network in the United States. It is a part of the INTERMAGNET. The USGS Geomagnetism Program currently operates 14 magnetic observatories. Magnetometer data are collected at these facilities. The data are then transmitted to Program headquarters in Golden, Colorado. The geographic distribution of the Program's observa-

tories, shown below (Figure 2.7), has been determined by the need to monitor and study the geomagnetic field on a global scale, primarily for purposes of space-weather diagnosis and main field modeling and mapping, as well as the practical issues of availability of land, communication, operational logistics, and the relative locations of observatories operated by other foreign-national programs.

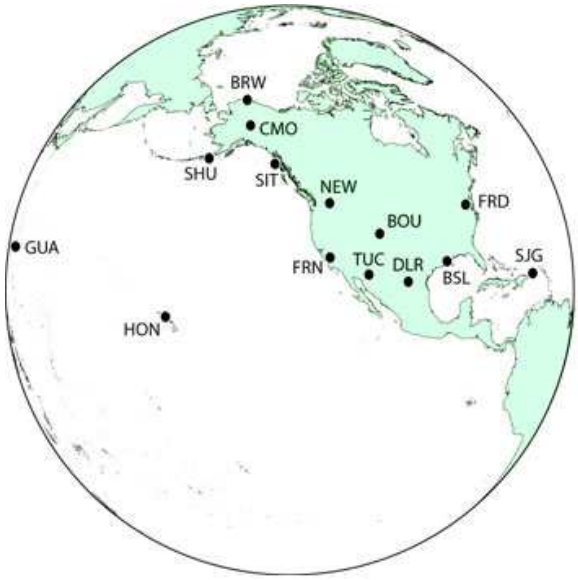


Fig. 2.7. The geographic distribution of the USGS observatories. (Downloaded from www.intermagnet.org.)

The data used in this dissertation research is provided by the INTERMAGNET and USGS. The time resolution is one minute. The magnitude resolution is 0.1 nT. The format is in HDZF format and XYDZ format. The XYDZ format data are converted into HDZF before applying wavelet analysis.

CHAPTER 3
RESEARCH APPROACH

In this dissertation research, several statistical and mathematic methods are applied to the geomagnetic data, including wavelet analysis, cross-spectrum correlation analysis and some other methods. The wavelet analysis is used to provide the basic spectral analysis for the geomagnetic data from single station and to decompose the data into different timescale variations for further study. The cross-spectrum correlation analysis is used to study the relationship between the geomagnetic data from different stations and to investigate the characteristics of the global symmetric and asymmetric components.

Wavelets are used as mathematical tools in a diverse set of fields, such as signal processing, medical imaging, pattern recognition, data compression, and numerical analysis. Basically, these applications can be categorized into image processing and time series analyzing. The application of wavelet analysis in time series analysis has been widely used in time series analysis for the last 20 years in areas such as seismology, finance, stock market studies, bio-information study, and space physics. It is also the mathematical foundation of this dissertation research.

3.1. Why wavelet?

Why is the wavelet analysis used in this dissertation study? The reason is as follows: The geomagnetic data contain variations of various spectral elements, which are related to complicated current systems in the ionosphere and magnetosphere. The goal of this study is the ring current. So we need to use a spectral analysis tool to decompose the original data into different frequency variations and still keep the localized information in time domain. The wavelet analysis is a suitable tool for such data with impulsive, multiscale, and nonstationary spectral features. It has a wide range of tools, such as wavelet transform, multiresolution analysis, timescale analysis, time-frequency representations, matching pur-

suit decompositions, and other powerful tools. It allows decomposing the geomagnetic data into the different timescales of variations, which are localized in time. This provides the possibility to separate the variations according to the timescales of their drivers, which are from the current systems in the ionosphere and magnetosphere. It also provides the possibility to reconstruct the data according to variations of specific timescales and frequencies after filtering process.

3.2. Comparison between wavelet transform and Fourier transform

As a tool to study spectra, wavelet analysis has similarities and dissimilarities compared to the Fast Fourier Transform (FFT), which is widely used in spectral analysis as a basic tool. They are both linear operations that generate a data structure that contains $\log_2(n)$ segments of various lengths, usually filling and transforming it into a different data vector of length 2^n. The mathematical properties of the matrices involved in the transforms are similar as well. The inverse transform matrix for both the wavelet transform and the FFT is the transpose of the original. As a result, both transforms can be viewed as a rotation in function space to a different domain. For the FFT, this new domain contains basis functions that are sines and cosines. For the wavelet transform, this new domain contains more complicated basis functions called wavelets, mother wavelets, or analyzing wavelets. Another similarity is that the basis functions are localized in frequency, making mathematical tools, such as power spectra (how much power is contained in a frequency interval), useful at picking out frequencies and calculating power distributions.

The most important dissimilarity between wavelet transform and Fourier transform is that individual wavelet functions are localized in space (time domain in geomagnetic data analysis). Fourier sine and cosine functions are not. This localization feature, along with wavelets' localization of frequency, makes many functions and operators using wavelet transform when transformed into the wavelet domain. This results in a number of useful applications such as data compression, detecting features in the original data, and removing noise from the time series, which is suitable for the geomagnetic data analysis.

Another advantage of wavelet transforms is that the windows vary. In order to isolate

signal discontinuities, one would like to have some very short basis functions. At the same time, in order to obtain detailed frequency analysis, one would like to have some very long basis functions. A way to achieve this is to have short high-frequency basis functions and long low-frequency ones. This provides the possibility of separate specific timescale of variations, which are contained in the original data.

3.3. Background of wavelet transforms

Wavelet is a small wave as its name suggests. A small wave grows and decays essentially in a limited time period. There are genders for wavelets: father wavelets ϕ and mother wavelets ψ. The father wavelet integrates to 1 and the mother wavelet integrates to 0:

$$\int \phi(t)dt = 1. \tag{3.1}$$

$$\int \psi(t)dt = 0. \tag{3.2}$$

The father wavelets are good at representing the smooth and low-frequency parts of a signal and the mother wavelets are good at representing the detail and high-frequency parts of a signal.

Generally, the wavelet transform can be categorized as the continuous wavelet transform (CWT) and the discrete wavelet transform (DWT). The CWT is designed to work with time series defined over the entire real axis. The orthogonal wavelet series approximation to a continuous time signal f(t) is given by:

$$f(t) \approx \sum_k S_{J,k}\phi_{J,k}(t) + \sum_k d_{J,k}\psi_{J,k}(t) + \sum_k d_{J-1,k}\psi_{J-1,k}(t) + \cdots + \sum_k d_{1,k}\psi_{1,k}(t), \tag{3.3}$$

where J is the number of multiresolution components (or scales), and k ranges from 1 to the number of coefficients in the specified component. The coefficients $s_{J,k}$, $d_{J,k}$, …, $d_{1,k}$ are the wavelet transform coefficients.

The functions $\phi_{J,k}(t)$ and $\psi_{j,k}(t)$ are the approximating wavelet functions, which are generated from ϕ and ψ through scaling and translation as follows:

$$\phi_{j,k}(t) = 2^{-j/2}\phi(2^{-j}t - k) = 2^{-j/2}\phi(\frac{t - 2^j k}{2^j}). \tag{3.4}$$

$$\psi_{j,k}(t) = 2^{-j/2}\psi(2^{-j}t - k) = 2^{-j/2}\psi(\frac{t - 2^j k}{2^j}). \tag{3.5}$$

The wavelet coefficients are given approximately by the integrals

$$S_{J,K} \approx \int \phi_{J,K}(t) f(t) dt \ , \tag{3.6}$$

$$d_{j,k} \approx \int \psi_{j,k}(t) f(t) dt, where, j = 1, 2, \ldots, J. \tag{3.7}$$

Their magnitude gives a measure of the contribution of the corresponding wavelet function to the approximating sum. The CWT includes orthogonal wavelet families, such as Daublets, Symmlets, Coiflets wavelets. The Daublets wavelets were the first type of continuous orthogonal wavelet with compact support. It is named in honor of its discoverer Ingrid Daubechies, who is one of the pioneers in wavelet research. The Symmlets also have compact support, and were also constructed by Daubechies. While the daublets are quite asymmetric, the Symmlets were constructed to be as nearly symmetric (or least asymmetric) as possible. The Coiflets were constructed by Daubechies to be nearly symmetric and also have additional properties thought to be desirable (vanishing moments for both ϕ and ψ). Daudechies used the name Coiflets in honor of Ronald Coifman, another important contributor to the theory and application of wavelet analysis.

The other main category of wavelet transform is the DWT, which deals with series

defined essentially over a range of integers (usually t= 0, 1, ..., N-1, where N denotes the number of values in the time series). The strength of DWT is in its perfect reconstruction and decorrelation properties and the fact that each DWT coefficient depends on only a limited portion of a time series, leading to the possibility of effectively dealing with time series whose statistical characteristics evolve overtime. The DWT can be considered as the subsampling scheme of the CWT. The DWT also efficiently collapses the two dimensional CWT back into a one dimensional quantity. The first DWT historically is the Haar DWT. The Haar wavelet is a square wave. It was discovered by the mathematician Haar in 1910 and provided the first known orthogonal wavelet series representations. The Haar wavelet has compact support, which means it is zero outside a finite interval. Though it is not continuous, it is the only compact orthogonal wavelet, which is symmetric.

A variation on the DWT called the maximal overlap DWT (MODWT) is used to decompose the geomagnetic record in this dissertation research. Like the DWT, the MODWT can be thought of as a subsampling of the CWT at dyadic scales; but, in contrast to the DWT, the MODWT can deal with all times t and not just those that are multiples of 2^j. In other word, the MODWT is more flexible on data span requirement. The geomagnetic records are not time series with multiples of 2^j, so the MODWT is more suitable for spectrum analysis than the DWT. Retaining all possible times can lead to a more appropriate summary of the CWT because this can eliminate certain alignment artifacts attributable to the way that the DWT subsamples the CWT across time.

An important concept of the wavelet transforms is the multiresolution analysis (MRA), which is defined as follows. We express the series X as the sum of a constant vector S_J and other vectors D_j, j=1, ..., J, each of which contains a time series related to variations in X at a certain timescale. The D_j is referred as the jth level wavelet detail.

$$X = \sum_{j=1}^{J} D_j + S_J \ , \tag{3.8}$$

where

$$S_J(t) = \sum_k S_{J,k}\phi_{J,k}(t) \ , \tag{3.9}$$

$$D_j(t) = \sum_k d_{j,k}\psi_{j,k}(t). \tag{3.10}$$

Figure 3.1 shows an example of decomposed geomagnetic records by applying MRA with the MODWT.

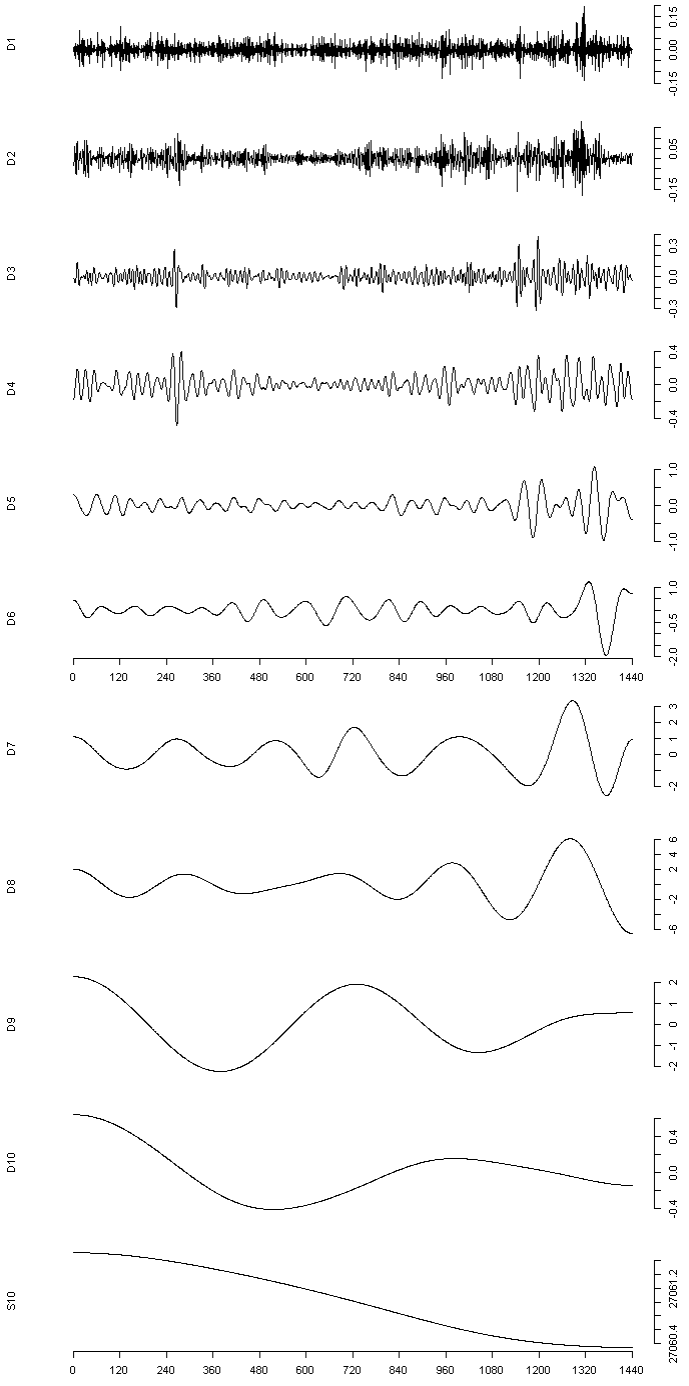


Fig. 3.1. Details (D1 to S10) of maximum overlap discrete wavelet transform (MODWT) for one quiet day (2001.01.05).

CHAPTER 4
AN ASSESSMENT STUDY OF THE WISA INDEX

In this chapter, a systematic assessment study of the WISA index is presented. First, we statistically compare the WISA with the Dst for both quiet and storm periods. Second, we analyze the differences of their spectral attributes by means of the Fast Fourier Transform. Third, we study the variability of the WISA when it is computed with data sets of varying length and from a varying number of stations. Lastly, we assess the WISA when it is calculated with artificial missing data. Our results show the hourly averaged WISA can describe the magnetic storm activities equally as well as the Dst and, more importantly, it can complement the traditional Dst with its fully automatic procedure, flexibility with data stretch, high temporal resolution, easiness of using the data from a varying number of stations, and high tolerance to missing data.

4.1. Dst index

A number of indices have been introduced to characterize the variations of specific current systems, including the Dst, AE, Kp indices, and recently a high-resolution index SYM-H. The Dst index was originally designed to describe the time variations of the ring current, which was thought to be symmetric around the Earth. More detailed information about the Dst index is introduced in a previous chapter.

One shortcoming of the Dst index is that several years of data are usually needed to produce the Dst index of good quality. To calculate the Dst index, one needs to determine the baseline for each observatory in which the secular variations and the Solar quiet (Sq) variations based on the five quietest days for each month are taken into account. Information about secular and Sq variations of the current year and the four preceding years is normally needed.

Another shortcoming of the Dst index is that it requires human intervention in its

calculation procedure. The five quietest days are determined manually at each observatory, and in the case of missing data, the data from a fifth station is needed and the manual interpolation is involved. These shortcomings of the traditional Dst method can lead to difficulties in its application to real-time monitoring of storm activities and space weather.

4.2. WISA index

To overcome these shortcomings in the Dst index, a Wavelet-based Index of Storm Activities (WISA) has been created by Jach et al. [28]. By applying the Maximum Overlap Discrete Wavelet Transform (MODWT) method to ground-based magnetometer data, the WISA can be automatically computed with a very flexible requirement on data stretch and it has a high tolerance for missing data. In addition, it has a much higher temporal resolution (one minute) than that of the Dst (one hour), which can better describe the dynamical variations of magnetic storm activities. The detailed description of the WISA index procedure can be found in [28].

In the automatic statistical procedure of the WISA index, we use a specific wavelet technique called Maximum Overlap Discrete Wavelet Transform (MODWT), which is a non-orthogonal modification of the Discrete Wavelet Transform (DWT). The MODWT addresses some shortcomings of the DWT, such as sample size restriction and sensitivity to the starting points of signal series. In the following, we provide a brief description of the WISA procedure.

First, the MODWT decomposes the horizontal magnetic field components into smoothes and details that represent the variations of different frequency levels in the recorded magnetic field. Second, the high-frequency noise, which is the small background variation (less than 0.2nT for level 1, less than 4nT for level 7 during the quiet period) in the high-frequency level details (level 1 to 7), is eliminated by wavelet thresholding using the quantile of 0.9 and the periodic variations associated with the Sq variations are filtered from the related details. Third, the long-term trend is subtracted from the smoothes. Then, all these details and smoothes are put together and form the output for a single station. Within this output, the noise, Sq, and trend variations have been removed from the horizontal magnetic field

components. Lastly, the quotients from all stations, which are obtained with dividing the variations with the cosines of their latitudes, are averaged to get the WISA index. More detailed information, as well as the mathematical formula, can be found in [28].

4.3. Comparisons between the WISA and the Dst indices

In section 4.2, we briefly described the statistical procedure of the WISA index. A natural question is how well the WISA represents the storm enhancements comparing to the Dst. In order to answer this question, we calculated the WISA index with magnetometer data from the four stations shown in Table 4.1 used in the Dst index calculations for the period of March-April, 2001. Then we compared the WISA with the Dst in terms of their statistical properties, including difference, correlation coefficients, and Root Mean Squared Errors (RMSE). The results are shown in Figure 4.1 and Figure 4.2.

Table 4.1. The four Dst stations.

Observatory	Geographic		Geomagnetic
	Longitude(E)	Latitude	Dipole Latitude
Hermanus	19.22	-34.40	-33.3
Kokioka	140.18	36.23	26.0
Honolulu	201.98	21.32	21.1
San Juan to January 1965	293.88	18.38	29.9

Figure 4.1 shows the WISA index, the Dst index, and the difference between them for the period of March and April in year 2001. Although the WISA index is calculated using

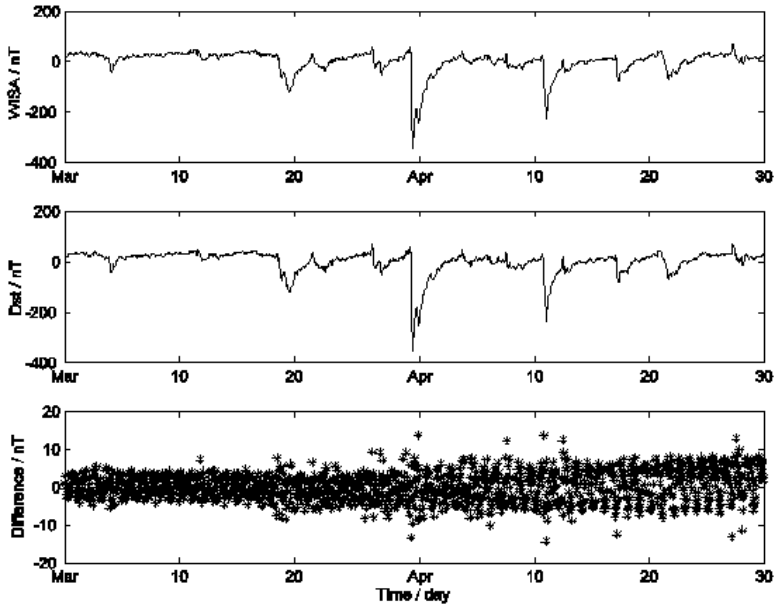


Fig. 4.1. The WISA index, Dst index, and their differences for the period March-April 2001.

the data from two months and the Dst index is computed with the data from more than one year, they are quite close to each other as shown in Figure 4.1. The difference between them is around 5 nT during quiet times, and the maximum difference is less than 15nT during storm times.

Figure 4.2 shows the correlation between the WISA and the Dst indices with a high correlation coefficient of 0.996. The results indicate the WISA and the Dst have a very good positive linear relationship. Another statistical property we checked is the Root Mean Squared Error (RMSE) between the WISA and the Dst indices. The definition of the RMSE is as follows:

$$RMSE = \sqrt{\frac{\sum_{i=1}^{N}(WISA(i) - Dst(i))^2}{N-1}}. \tag{4.1}$$

The RMSE is a measure of the typical distance between the WISA and the Dst indices. The RMSE between the WISA and Dst indices for this period is 3.820nT. Such a

small RMSE, comparing to the maximum magnitude of the storm, which is about 400nT, shows the WISA index varies closely to the Dst index variations through the whole period of March-April 2001, even though there existed a very strong storm. Furthermore, we compared the WISA and the Dst indices for quiet periods by using the data from July-August in year 2001. The results show the WISA and the Dst indices are still very close to each other with the difference around 10nT except for the storm on August 18 where the difference is between 10nT and 20nT. The correlation coefficient is 0.978, and the RMSE is 2.812nT for this period.

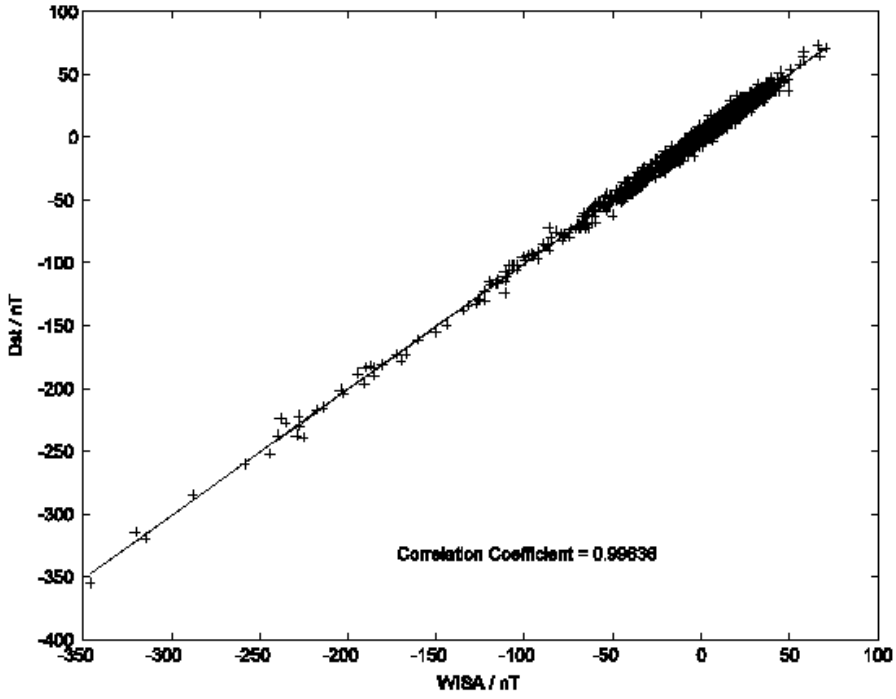


Fig. 4.2. The scatter plot of the WISA and Dst indices for the period of March-April 2001.

From the two cases described above, we can see the WISA index is as good as the Dst index for describing the variability of the geomagnetic conditions for both storm and quiet times, but with the strength of full automation. In addition, we also compared the WISA and Dst for the whole of 2001. The results are similar to those shown in above paragraphs, which have a high correlation coefficient (0.993), low RMSE (3.951nT), and small difference

(between -20nT and 20nT). More comparisons between the WISA and the Dst indices for different periods of time are shown in section 4.5 when we assess the flexibility of the WISA on data stretch.

4.4. FFT analysis on the WISA and Dst indices

In the previous section, we showed the WISA can describe the geomagnetic activities of both the storm and quiet times equally well as the Dst. In order to get further details about the difference between them, we used Fast Fourier Transform (FFT) analysis to study their spectral features, with the focus on the frequency band of the Sq variations.

One of the most important steps in both the WISA and Dst procedures is removing the Solar Quiet daily (Sq) variations. We applied the Fast Fourier Transform (FFT) analysis to the WISA index, the Dst index, and the difference between them to quantitatively assess how well they remove the Sq components. Figure 4.3 shows the results of these FFT analyses. We can see the FFT results of the WISA index and the Dst index are quite similar, but there are some peaks in the FFT result of the difference. Those peaks are 24-, 12-, 8-, and 6-hour period peaks. These peaks could come from the different methods of removing the Sq variations in the two indices. A detailed explanation follows.

In the method of removing the Sq variations used by the Dst index, the average Sq variation for each month is first determined from the values of H component by hours for the internationally selected five quietest days of the month. Then the averages for the local hours are formed by using five local days that have the maximum overlap with the international five quietest days. And the Sq is expanded as a double Fourier series in the local time (LT) T and month number M,

$$S_q(t,s) = \sum_m \sum_n A_{mn} cos(mt + \alpha_m) cos(ns + \beta_n). \tag{4.2}$$

The series contain 48 unknown coefficients A_{mn}, α_m, and β_n. These are determined by computing one Sq curve for each month as an average of the variation curves of the five quietest days of the month. If for a specific month, there are no ideal quiet days, the

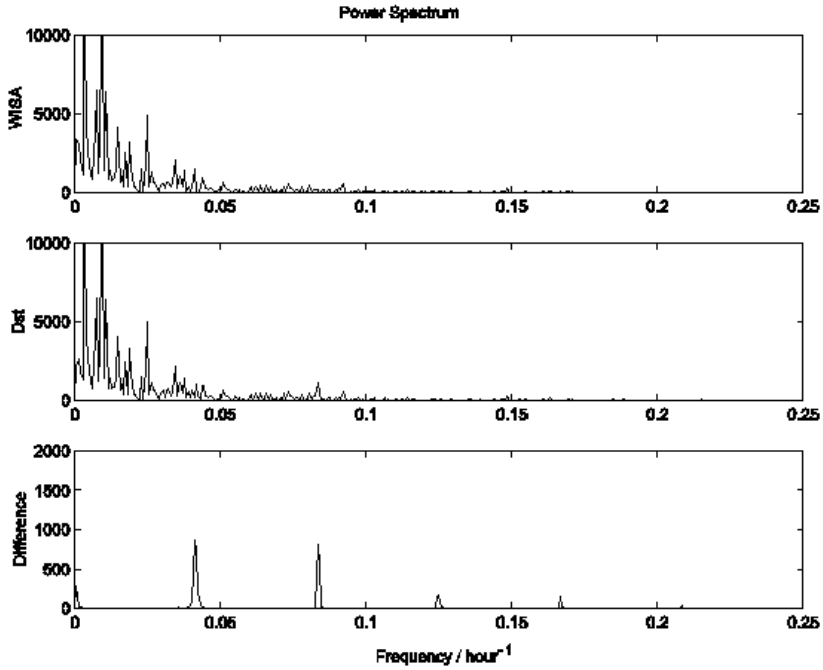


Fig. 4.3. The FFT results of the WISA, Dst indices, and their difference for the period of March-April 2001.

data from the same month of the preceding years are used. Since the five quietest days are decided manually, the procedure of removing the Sq variation needs human action for the Dst index and a multi-year long data stretch in some situations.

In the method of removing the Sq variations used by the WISA index, the details referring the Sq variations are filtered to remove periodical components. This is done in one-minute resolution. Then the hourly medians are calculated for the current data stretch. There is no need to determine hourly data of the five quiet days before the subtractions of Sq variations as that in the Dst. For Figure 4.3, only the data from March-April of year 2001 are used.

More details of the residues of Sq variations in the WISA are studied by checking the Inverse Fast Fourier Transform (IFFT) for the periods of these peaks. We select the same wide waveband near each peak in the frequency domain and transform them into the time domain by IFFT. In Figure 4.4, the top part is the WISA index during March-April 2001; the other four subplots are the inverse components of 24-, 12-, 8-, and 6-hour peaks during

this period. All the components of IFFT of 24-, 12-, 8-, and 6-hour peaks in the WISA index are less than 2 nT; therefore, the periodical residues of Sq variations are quite small and insignificant in the WISA.

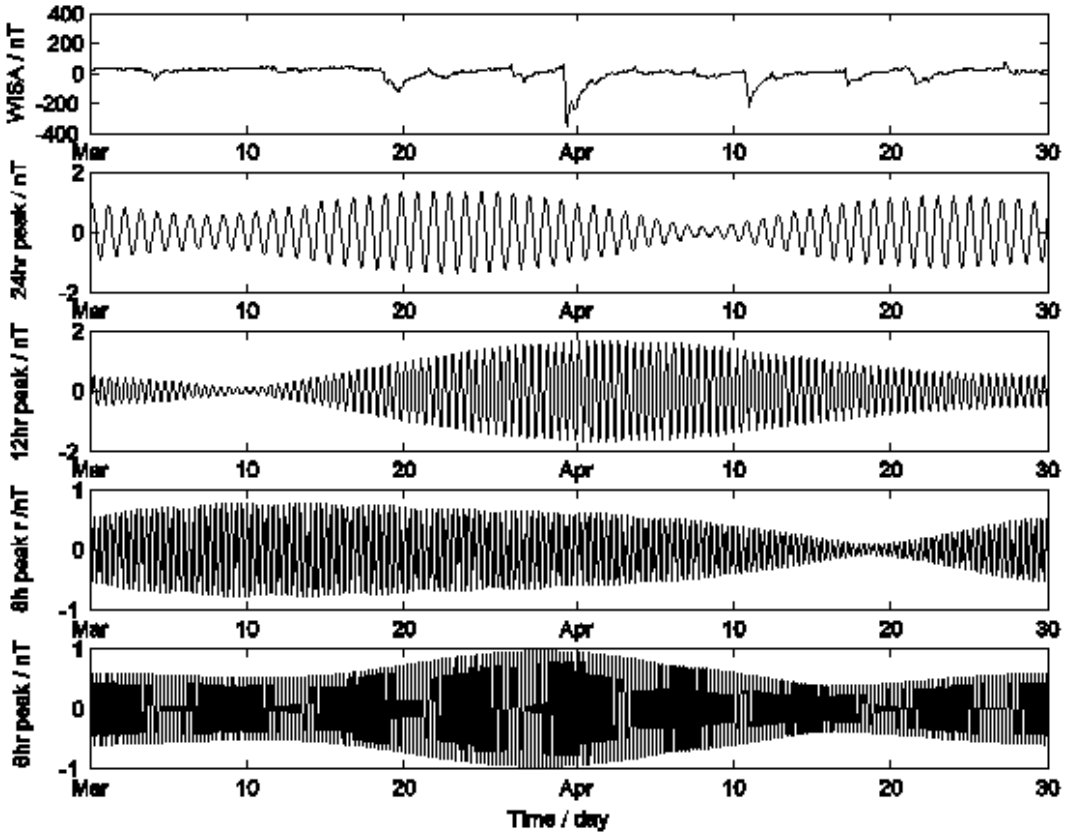


Fig. 4.4. The WISA index and the inverse FFT peak components of 24-, 12-, 8-, and 6-hour periods for the period of March-April 2001.

In the above, both the FFT and the IFFT results show although the WISA index removes the Sq variations automatically with flexible data stretch, the residues of the Sq variations are on the same level as that of the Dst index, which uses a procedure with human actions and long data stretch. The different methods used by the WISA and Dst to remove the Sq components may cause a small difference of their Sq residues and, at this point, it is hard to quantitatively determine which one is cleaner with respect to removing the Sq variations.

4.5. Flexibility of the WISA on data stretch

After comparing the WISA with the Dst on their spectral features, we statistically assess the flexibility of the WISA on data stretch. The high flexibility on data stretch is one of the strengths of the WISA. The procedure based on the wavelet transform makes it possible to automatically remove the Sq variations from even a short data stretch, while the procedure of the Dst index requires the five quietest days for every month, which are determined manually from a long data stretch, in most cases, over one year. To assess this, we calculate the WISA index with data stretches of different lengths, including one year of data, one month of data, and even as little as eight days of data, then compare them with the Dst index. The results are as follows.

Figure 4.5 shows an extreme case of these comparisons, in which the WISA index calculated with an eight-day data set is compared to the Dst index that was calculated using more than one year of data. In Figure 4.5, the WISA index is very close to the Dst index, the difference between the WISA and Dst indices is smaller than 10 nT during quiet-time periods, and is less than 20 nT during storm-time periods.

Figure 4.6 shows the correlation between the WISA and Dst indices and the correlation coefficient is 0.998. They have an almost perfect positive linear relation. We also calculated the RMSE between the two indices and it is 5.255nT, which is quite good considering the existence of a strong storm of over 200nT during these eight days.

Table 4.2 shows the results of statistical comparisons between the WISA indices calculated with different data stretches and the Dst index. The WISA and Dst indices still have highly positive linear relation for all these different data stretches. The range of difference between them is between -20nT and 20nT. The RMSE results are smaller than 5.5nT, which means the deviations between the WISA and Dst indices stay small.

From the above results, we can conclude the WISA indices calculated with various data stretches work as well as the Dst for describing the enhancements of geomagnetic field H component during storm and quiet periods. The difference between them is always small, the RMSEs are on the order of a few nTs, and the correlation coefficient is close to one.

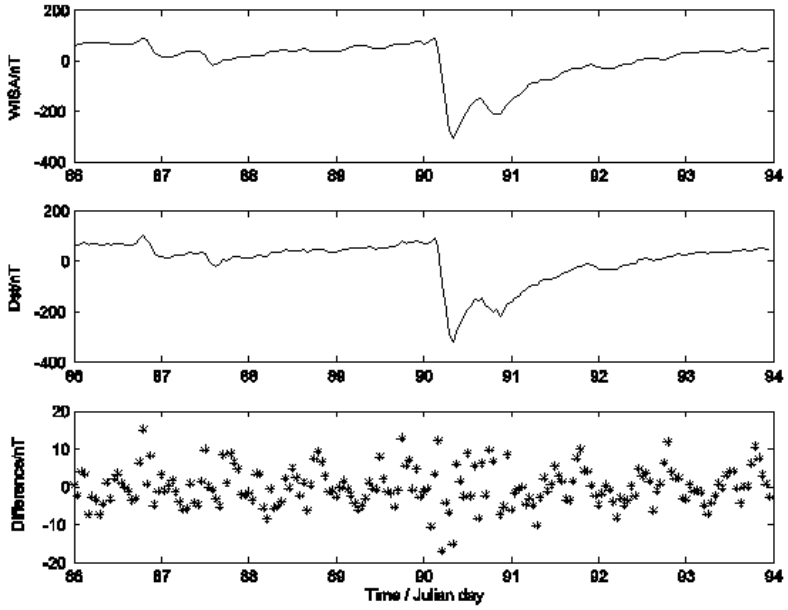


Fig. 4.5. The WISA, Dst indices, and their difference for the Julian days 86-93 in year 2001.

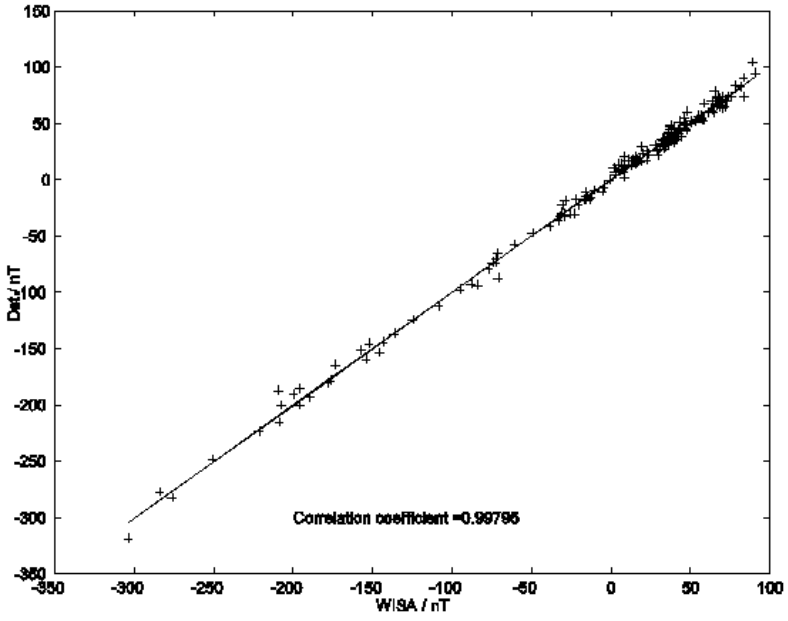


Fig. 4.6. The scatter plot of the WISA and Dst indices for Julian days 86-93 in year 2001.

Table 4.2. Statistical comparisons between the WISA index calculated on different data stretches and the Dst index.

Time periods	Range of Difference (nT)	Correlation Coefficient	RMSE
Year 2001	(-20,20)	0.99258	3.9505
2001.month.03-04	(-15,15)	0.99636	3.8198
2001.month.07-08	(-10,20)	0.97798	2.8123
2001.day.75-104	(-20,20)	0.99632	4.7880
2001.day.86-93	(-20,20)	0.99795	5.2546

The difference between the two indices' procedures is the Dst index is calculated with at least one year of data, but the WISA can be calculated by even as short as eight days of data and still have the same quality as the Dst for describing geomagnetic variations. The procedure of the WISA, which can use much less data than the Dst, makes it possible to serve as a real-time index for space weather applications.

4.6. Effects of varying number of stations on the WISA

In addition to the automation and the flexibility on data stretch discussed in previous sections, another assessment on the WISA is the study of effects of varying number of stations on the index calculation. This study can answer a question that is frequently asked for the Dst index, "how many stations are needed for a well-behaved Dst index?" [39]. Actually, the official Dst index procedure changed the required number of stations in the calculation procedure several times. The current Dst uses four stations. The hourly Dst values for the IGY (1957-1958) were based on the data from eight stations. The hourly

values of the Dst for the years 1957-1970 were based on the data from three stations. Since the Dst procedure needs data of more than one year, it is difficult to study the effects of varying number of stations on the Dst index. For the WISA index, it is easy to study the effects of varying number of stations because its automation allows us to apply the WISA procedure to different stations easily.

First, we selected ten stations, which consist of four original Dst stations and six low-latitude stations (listed in Table 4.3), and we tried to make the longitudinal distribution of the stations as uniform as possible. Then we processed the data for the period of March-April of 2001 with the WISA procedure to calculate the H component enhancements and corrected them with their locations.

Second, we separated the stations into different groups and created the WISAs of varying number of stations by averaging the H component enhancements in each group. For example, the two-station WISA means the average of two station results. The combinations of stations used for studying the effects of varying number of stations on the WISA are shown in Table 4.4. The stations are grouped as symmetrically as possible.

Then, the data of 10 stations are used to calculate the 10-station WISA, and the 10-station WISA is compared to the Dst index for the period of March-April 2001. Figure 4.7 shows the WISA, Dst indices, and the difference between them. The WISA index has almost the same shape as the Dst index. The difference between them is small (around 10nT) during the quiet-time periods, but increases to 60nT during the storm period. The reason behind this is the current systems contributing to the magnetic field variations around equatorial region are strongly asymmetric. Although, in the equatorial region, the ring current system is assumed to be symmetric and is a primary contributor to geomagnetic field H component enhancements. There are also several local time-dependent current systems contributing asymmetrically to the geomagnetic field enhancements. When geomagnetic activities are quiet, the asymmetric enhancements are small compared to the contribution of the ring current system. However, when the geomagnetic activities move to storm level, the local time-dependent current systems increase their contributions to the enhancements

Table 4.3. The list of stations used for studying the effects of varying numbers of stations on the WISA.

Code	Name	Colatitude	East Longitude
ABG	Alibag	71.38	72.87
HER	Hermanus	124.43	19.23
HON	Honolulu	68.68	202.00
KAK	Kakioka	53.77	140.18
MBO	Mbour	75.62	343.03
MID	Midway Island	61.79	182.62
PHU	Phuthuy	68.97	105.95
SJG	San Juan	71.89	293.85
TAN	Tamanrasset	108.92	47.55
TUC	Tucson	57.82	249.27

of geomagnetic field H component. The Dst index, which use the observations of four stations is not capable of fully picking up the local enhancement component, while the 10-station WISA can.

Table 4.4. The combinations of stations used for studying the effects of varying numbers of stations on the WISA.

Name	Combinations
2a-station	KAK,SJG
2b-station	HER, HON
3a-station	HON, KAK, SJG
3b-station	HER, HON, SJG
3c-station	HER, HON, KAK
3d-station	HER, KAK, SJG
4-station	HER, HON, KAK, SJG
8a-station	ABG, KAK, MBO, MID, SJG, PHU, TAN, TUC
8b-station	ABG, HER, HON, MBO, MID, PHU, TAN, TUC
10-station	ABG, HER, HON, KAK, MBO, MID, SJG, PHU, TAN, TUC

We calculated the WISA index with the data from two, three, and eight stations, and compared the results with 10-station WISA for three different time periods. These time periods are March-April, 2001, quiet time from March 5 to 12, 2001, and storm time from

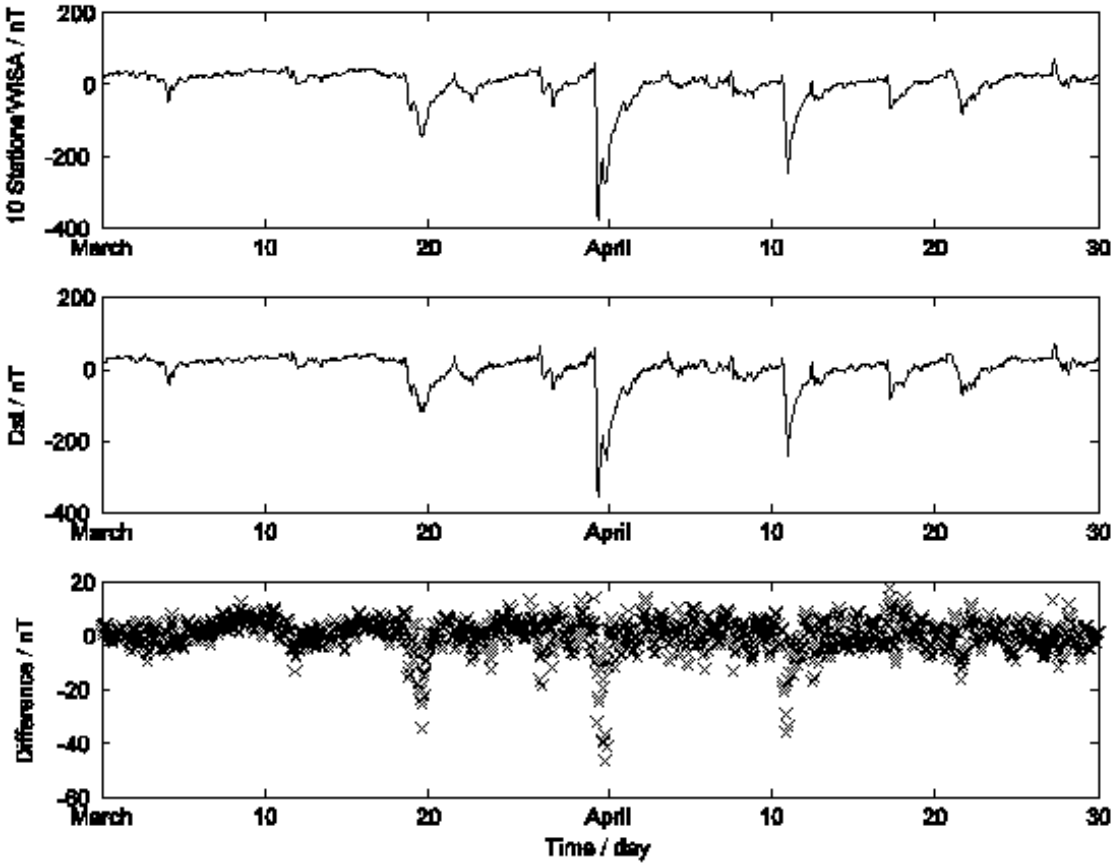


Fig. 4.7. The 10-station WISA, the Dst and the difference between them for the period of March-April 2001.

March 27 to April 5, 2001. The results are shown in Table 4.5. According to these differences and RMSE results, we can tell when the number of stations used in the WISA calculations increases, the results are closer to the 10-station WISA. The difference and RMSE during the quiet-time periods are smaller than those during storm-time periods. This is the evidence that the asymmetric enhancements of geomagnetic field H component are stronger during storm times than quiet times.

The study of the WISA with the data from varying number of stations shows there exist asymmetric behaviors of the enhancements during geomagnetic disturbing periods. Data

Table 4.5. The difference and Root Mean Squared Errors (RMSE) between 10-station WISA and other numbers of station during March-April, 2001, the quiet time, and the storm time in that period.

Station Combinations	March-April 2001		Quiet time (03/05-03/12/2001)		Storm time (03/27-04/05/2001)	
	Range of Difference	RMSE	Range of Difference	RMSE	Range of Difference	RMSE
2a	(-20,60)	7.6312	(-15,10)	6.8474	(-20,60)	10.9111
2b	(-20,40)	6.3883	(-15,10)	4.5583	(-20,40)	9.7553
3a	(-30,70)	7.4707	(-15,15)	5.756	(-10,70)	10.5108
3b	(-20,40)	5.8194	(-10,15)	4.8229	(-20,40)	8.0552
3c	(-20,60)	6.5268	(-15,15)	5.0136	(-20,60)	10.4886
3d	(-20,70)	6.1322	(-15,10)	5.5164	(-20,70)	9.7718
4	(-20,50)	5.2599	(-12,8)	4.8467	(-20,40)	8.1278
8a	(-10,6)	1.5971	(-3,4)	1.1396	(-10,6)	2.4388
8b	(-14,6)	1.9078	(-3,5)	1.7118	(-14,6)	2.7278

from four stations are not sufficient for detecting these local time-dependent components. Data from eight stations may be sufficient to pick up the local enhancement components. The study also shows the asymmetric behaviors of the geomagnetic field are stronger during storms than quiet-time periods since the local time-dependent components are significantly enhanced by storms. All these studies are based on the convenience of the WISA automatic procedure with flexible data stretch.

4.7. Effects of missing data on the WISA

With the statistical nature of the wavelet method, the WISA index can handle the data set with missing data automatically while the Dst index has to use additional observations with human intervention. In this section, the effects of missing data on the WISA are assessed by calculating the WISA index with the data sets having artificially missing data of various lengths and positions.

In order to make the periods with artificial missing data more realistic, we went through the real data of all four Dst stations for 2001 to find out the real distribution of missing data. In fact, Station Kakioka (KAK) and Station Hermanus (HER) have no missing data and the missing data distributions of Station San Juan (SJG) and Station Honolulu (HON) are shown in Figure 4.8. According to Figure 4.8, the distribution of missing data is as follows: for one-minute period, less than 50 times per year; for 10-minute period, less than 24 times per year; for 30-minute period, less than 10 times per year; for one-hour period, less than 10 times per year; for three-hour period, less than 10 times per year; for 12-hour period, less than 10 times per year; and for over 24-hour period, less than five times per year. To realistically simulate missing data, we artificially created various periods of missing data during the months of March and April, 2001 for which KAK station has no missing data. The artificial missing data periods are 10 of one minute, two of 10 minutes, two of 30 minutes, one of one hour, one of three hours, one of 12 hours, and one of 24 hours. The resulted WISA are compared with the WISA calculated with the data without artificial missing data and the comparison results are shown in Table 4.6.

Table 4.6. Missing data effects during quiet time.

Periods of Artificial Missing Data	10 of 1 minute	2 of 10 minutes	2 of 30 minutes	1 of 1 hour	1 of 3 hours	1 of 12 hours	1 of 24 hours
Range of Difference	(-0.0025,0.0005)	(-0.007,0.001)	(-0.24,0.1)	(-0.05,0.35)	(-0.2,1.8)	(-0.5,3)	(-2,12)
Correlation Coefficients	1	1	1	1	1	1	0.99992
RMSE	0.0002385	0.00030874	0.0063879	0.012001	0.067746	0.12103	0.54814

The WISA handles the missing data with the periods shorter than three hours quite well with its wavelet statistical procedure. The result of 12 hours missing data is still good for such an index that mainly describes the enhancements of geomagnetic field H component during storm time and the disturbances are normally above 50nT. The result of 24 hours missing data is noticeably different from the WISA without artificial missing data, but the chance of such a long period of missing data is only once in a year.

The above artificial missing data are mostly in the quiet-time periods. Since the WISA index is mainly used for storm activities, we also studied the effects of missing data during storm-time periods. For the storm period from March 27 to April 5, 2001, we applied the same types of artificial missing data periods which we used for quiet periods, and repeated the same calculations as above for a missing data period of 24 hours. The comparisons between the WISA with artificially missing data during storm-time periods and the WISA without artificial missing data are shown in Table 4.7.

In Table 4.7, the differences and RMSEs increase by nearly one order compared to the results for quiet-time periods. The results are still good for missing periods of less than 3 hours, but for the periods over 3 hours the difference are significant. In reality, the storm-

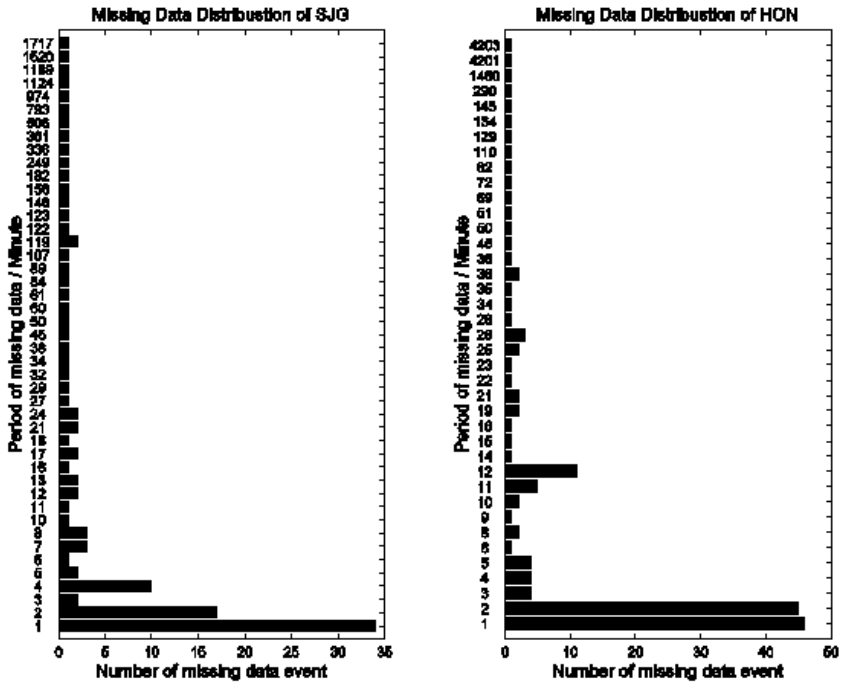


Fig. 4.8. Missing data distributions of geomagnetic observatories SJG and HON in year 2001.

Table 4.7. Missing data effects during storm time.

storm	01min	10min	30min	01hour	03hour	12hour
Range of Difference	(-0.018,0.002)	(-0.02,0.03)	(-0.2,1.2)	(-2,0.5)	(-2,12)	(-25,10)
Correlation Coefficients	1	1	1	1	0.99998	0.99955
RMSE*	0.00061076	0.00095983	0.02546	0.052071	0.31832	1.4333

time periods are much less than quiet-time periods, so the occurrence of the situation shown in Table 4.7 should be very rare.

In general, the WISA can automatically handle the missing data without human intervention while the Dst index needs additional data from a fifth station and manual interpolations. The WISA is still reliable for missing data less than 12 hours for quiet-time periods since both the average of difference amplitude and RMSE are small and the correlation show almost perfect linear relations. For storm-time periods, the WISA behave well when the periods of missing data are less than 3 hours, but such a long period of missing data happens rarely during storm time. The automation of handling missing data makes is another strength of the WISA over the Dst and it is one of the crucial features for an index to be used to monitor the real-time space weather conditions.

4.8. Discussions and conclusions

In this chapter, we performed a systematic quantitative assessment study on the Wavelet-based Index of magnetic Storm Activity (WISA) and statistically compare the WISA index to the Dst index with the data from various periods under various conditions. By using a wavelet-based statistical procedure, the WISA index can be calculated automatically without human intervention with very flexible data stretch. The results show the WISA index can do equally well as the Dst index for describing the variations of geomagnetic field during both storm and quiet periods, but in addition, it has higher temporal resolution, ability of using data from varying number of stations, and high tolerance on missing data. The detailed quantitative assessment results are as follows:

a. The comparisons between the WISA and Dst indices show the difference between the two are consistently below 10nT for quiet times and below 20nT even for major storms. The statistical correlation between the two has a very good linear relationship with a correlation coefficient close to 1. The statistical deviation is very small and the values of Root Mean Squared Errors (RMSE) are between 3.8nT and 3.9nT. All these statistical results clearly indicate the WISA describes the storm time enhancements equally well as the Dst.

b. The results of the Fourier transform analysis of the WISA and Dst indices show the

spectral features of the two indices are very similar, but there are some small peaks in the differences of the two indices in spectrum domain. These peaks may be due to the different approaches of removing the components of Sq variations in two indices. The inverse FFT results of the WISA show the residues of the Sq variations in the index are minimal, which is around 2nT.

c. The results from comparing the WISA calculated with varying data stretches (one year, two months, one month, and eight days) to the Dst show the WISA indices are always highly correlated with the Dst index with correlation coefficients larger than 9.8 and a very small statistical deviation from the Dst. This proves the WISA has a good flexibility on data stretch, and in contrast, the Dst may need multi-year data to produce the index of the same quality.

d. The study on the effects of varying number of stations on the WISA shows the Dst index, which traditionally uses the data from four low-latitude stations, may not be able to sufficiently pick up the local enhancement component. Eight stations can do a much better job. The results also show the asymmetric enhancements of geomagnetic field H component can become significant during the storm-time periods.

e. The tests of computing the WISA with artificially missing data show the WISA procedure can reasonably tolerate the missing data for less than 12 hours during quiet-time periods and less than 3 hours during storm-time periods.

This assessment study of the WISA index and its statistical comparisons to the Dst provides a clear quantitative picture on the quality and strengths of the WISA and its advantages over the Dst. These quantitative information would be very useful for applying the WISA method to the future studies of geomagnetic activities. With its fully automatic procedure, high flexibility on data stretch, convenience of using data from varying number of stations, high temporal resolution, and high tolerance for missing data from individual station, the WISA can be very useful and essential for real-time monitoring of the dynamical variations of magnetic storm activities and space weather applications.

CHAPTER 5
WAVELET CROSS-SPECTRUM ANALYSIS OF THE RING CURRENT USING MAGNETIC RECORDS FROM MULTIPLE LOW-LATITUDE STATIONS

In the previous chapter, we perform an assessment study on the strengths of applying the wavelet procedure to geomagnetic data for ring current study by comparing a wavelet-based storm index with the Dst index. In this chapter, we study the characteristics of symmetric and asymmetric components of the ring current by using the decomposed and filtered geomagnetic records with wavelet analysis.

5.1. Introduction of symmetric and asymmetric components of the ring current

In order to describe the symmetric and asymmetric components in the ring current, several indices have been developed. The symmetric components of the ring current are reflected by global symmetric enhancements of geomagnetic activities in equatorial regions, which are presumably described by the Dst index. The Dst was originally designed to describe the variations of the symmetric ring current. But, over the years, it has been a consensus of the space science community that with the specific Dst derivation procedure, the index actually has significant components of the asymmetric ring current and other local-time dependent currents [23], [38], [40]. By using both low- and mid-latitude magnetometer data, a set of high-resolution indices, SYM-H and ASY-H, were developed later [41] and used by the community [20] [26] to describe the variability of the symmetric and asymmetric parts of the ring current. Because the SYM-H and ASY-H use a similar approach as the Dst to eliminate the Sq current effect, which is simply based on the data of the five quietest days of the month, the separation of the magnetic effects of the symmetric and asymmetric parts of the ring current in the SYM-H and ASYM-H indices is basically on the same level as in the Dst, and there is a significant cross-contamination between the SYM-H and ASY-

H. Separating the magnetic effects of the symmetric and asymmetric components of the ring current is still an unsolved issue, and an ongoing scientific task for the space science community. The study of the variability of the symmetric and asymmetric ring currents separately would greatly improve our understanding of the dynamics of the M-I current system.

In this chapter, the H components of magnetometer data are decomposed into different levels of details by using a specific wavelet transform and a systematic study of the temporal and frequency properties of the magnetic disturbances for various geomagnetic and seasonal conditions is performed. Then the wavelet cross-spectrum analysis on the data from multiple stations is conducted, in both UT (Universal Time) and LT (Local Time) frames, to separate and elucidate the magnetic effects of the symmetric and asymmetric parts of the ring current.

5.2. Data and method

The magnetometer data are selected from four geomagnetic observation stations, which are also used to produce the Dst index. The locations of these stations are shown in Table 5.1 and they are basically longitudinally symmetric in the equatorial regions. The data are in one-minute time resolution and cover the whole year of 2001. The data from SJG, KOK, HON are formatted in HDZ components, but the data from HER are formatted in XYZ components, where the H is the horizontal component, the D is the declination angle, the Z is the vertical component, the X is the north component, and the Y is the east component. We use the H components in our spectrum study, therefore the X and Y components of the HER data need to be converted into the H component. Two quiet periods are selected from the database, which are 2001.01.05-01.19 and 2001.06.22-07.07. Two storm periods (2001.03.18-04.03 and 2001.10.15-10.30) are also selected for our study. The Dst index is used for choosing quiet and storm periods as shown in Figure 5.1. The Dst index is overall in the range of 30nT for quiet periods. For storm periods, the Dst has several disturbances, which have magnitudes over 50nT.

Table 5.1. The locations of four Dst Stations.

Observatory		Geographic		Geomagnetic
Names	3 letter ID	Longitude(E)	Latitude	Dipole Latitude
Hermanus	HER	19.22	-34.40	-33.3
Kokioka	KOK	140.18	36.23	26.0
Honolulu	HON	201.98	21.32	21.1
San Juan	SJG	293.88	18.38	29.9

For wavelet analysis, the same wavelet technique as in Chapter 4, Maximum Overlap Discrete Wavelet Transform (MODWT), is chosen to transform the H components of geomagnetic data into different frequency levels of variations which are called details and smoothes. Since the different details are related to the frequency variations of different timescales after the MODWT decomposition, the geomagnetic variations connected with these details are separated by the frequencies of their sources. The linear correlations of these variations from different geophysical locations are compared in different time frames to investigate whether they are globally symmetric or asymmetric.

The following is an example of wavelet analysis for the H component of magnetometer data. Figure 5.2 shows the details of the one-day H component from SJG station after applying the MODWT. Different frequency variations are represented by different Details. Detail 1 (D1) to Detail 10 (D10) are related to the variations of the periods from 2-4 minutes to 210-211 minutes (about 17-34 hours). The Smooth 10 (S10) is the rest of the H component excluding all the details and shows the slow varying component in the one-day variation. If all these details and smoothes are summed together, the original H component

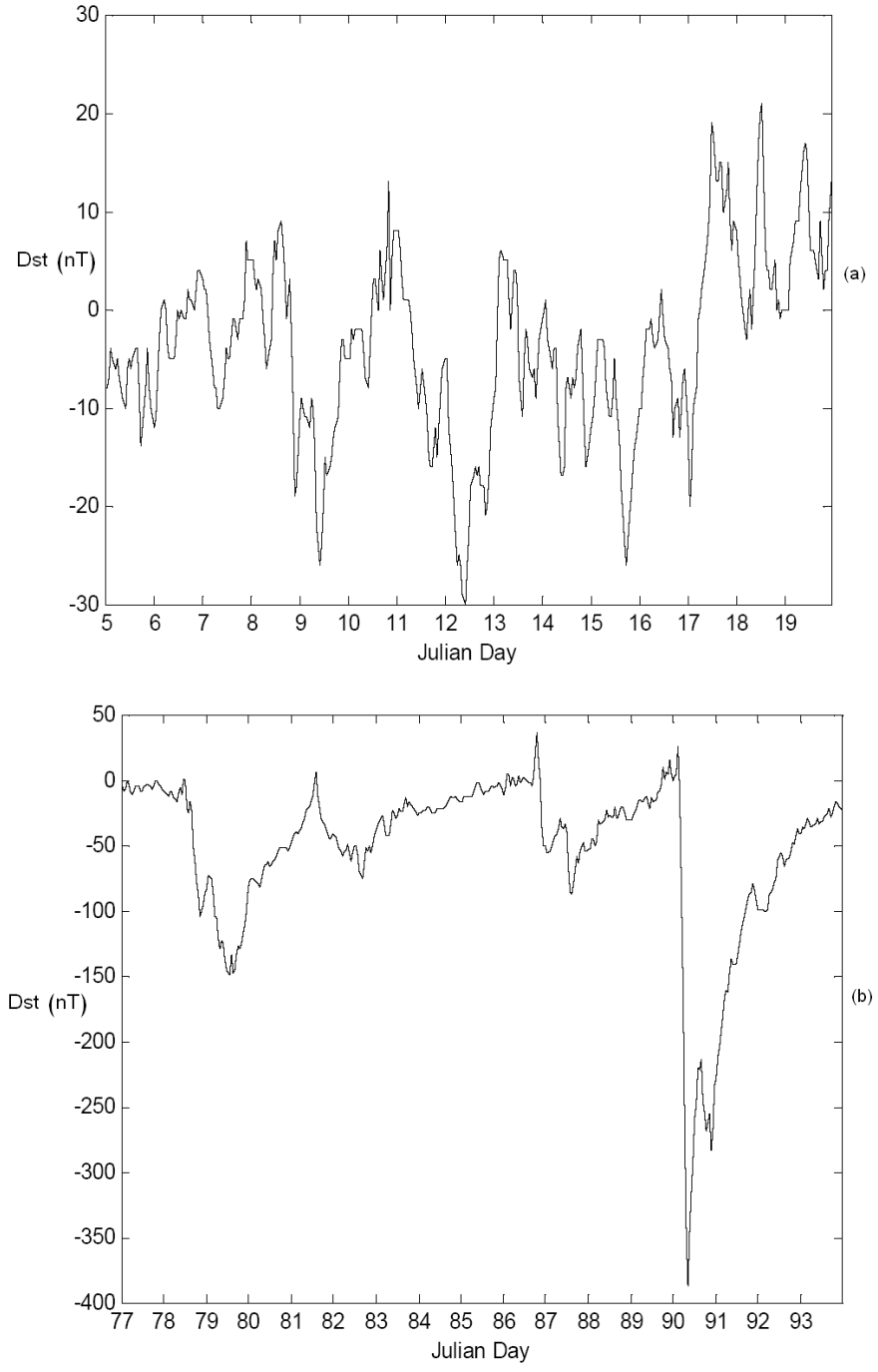


Fig. 5.1. The Dst index for the quiet period (a) (2001.01.05-01.19), and the storm period (b) (2001.03.18-04.03).

is recovered. Figure 5.2 clearly shows properties of the details change in time. In this chapter, we study the temporal and frequency properties of the magnetic disturbances for various geomagnetic and seasonal conditions.

The cross correlation analysis, which means the linear correlation coefficients are calculated across the same level details between different stations, is applied to the MODWT details. Both universal and local timeframes are used in the cross correlation studies. Since the four geomagnetic stations are chosen, there are six pairs of comparison for either UT or LT frames. For the LT frame, the data are shifted to LT zero of SJG station in this chapter. The reason the cross-correlation analysis is performed in both UT and LT frames is the global symmetric components should have greater correlations in the UT frame and the asymmetric components should have greater correlations in the LT frame. The comparison of correlations on different levels of details can show how symmetric and asymmetric components behave in terms of different frequencies. The comparison for quiet and storm periods can demonstrate how the symmetric and asymmetric components vary from quiet to storm periods. Additionally, the magnitudes of different details are analyzed and compared with each other. The average magnitudes of each station are calculated by summing absolute values and dividing by the time span for each case. These results present the difference of magnitudes among different details and stations during quiet and storm periods. Since the details are related to different frequency variations, the greater magnitudes of details show the stronger variations. It also indicates the strengths of magnetic disturbances for quiet and storm periods.

5.3. Results

5.3.1. Quiet periods study (2001.01.05-01.19 and 2001.06.22-07.07)

After decomposing the magnetometer data with the MODWT, the same level of details from different stations are put together in the UT frame and compared systematically. Similar patterns are found in the details above D11 in Figure 5.3. These patterns vary approximately in phase in the UT frame. There are peaks around the same times in all

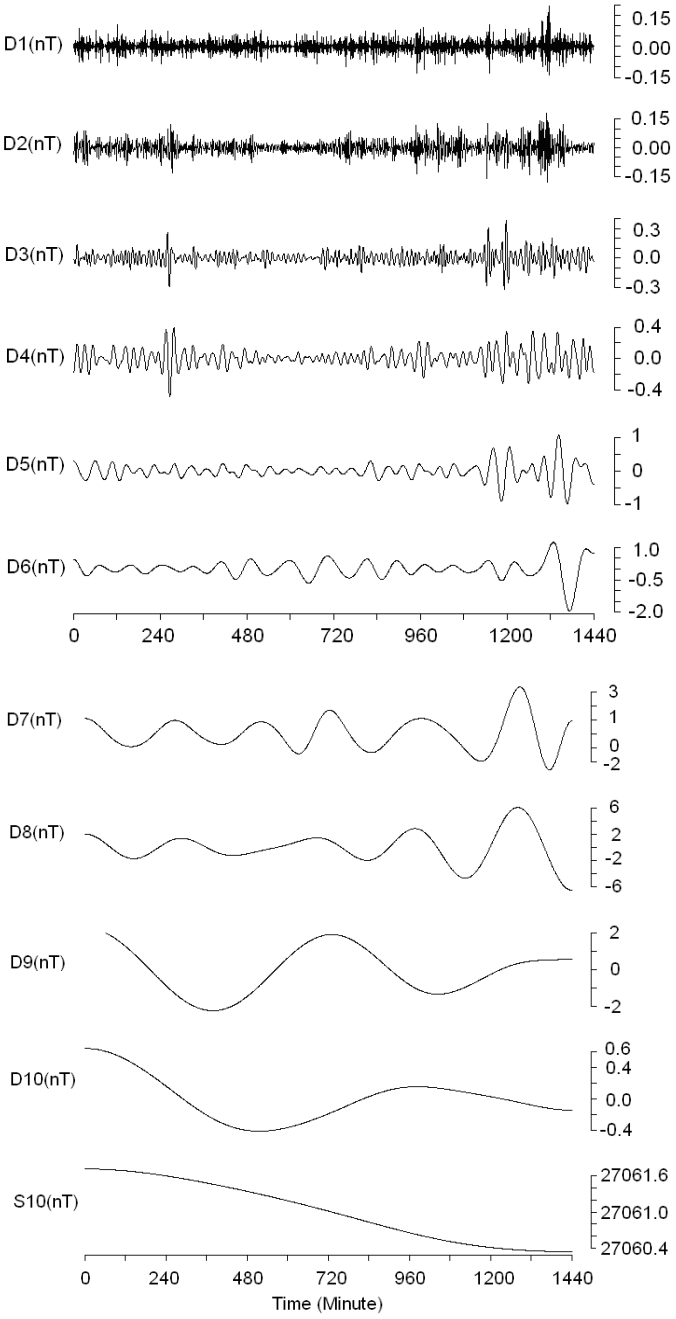


Fig. 5.2. MODWT Details (D1-D10) and Smooth (S10) for one quiet day (2001.01.05).

four stations during day 10 and 14 in D11 and D12 as shown in Figure 5.3. The in-phase disturbances observed by all four equatorial stations indicate these are global symmetric components that are from the enhancements of the symmetric ring current.

The details of D8, D9, and D10, which are close to diurnal variation, are also compared in the UT frame as shown in Figure 5.4. These are complicated patterns that are connected with different local-time dependent sources, such as the Sq variation, substorms, tail current, and partial ring current. The Sq variation contributes to the diurnal variations. The tail current contributes to the night-side variations. The substorm effect lasts several hours. These effects form the complicated patterns showed in Figure 5.4 and these are asymmetric components or local-time dependent components.

Because the visual inspection does not provide quantitative information, the cross correlation analysis is applied to get further information from different levels of details and to investigate the symmetric or asymmetric relationship between them. The cross correlation analysis means we calculate the correlation coefficients between the details at the same levels across different stations. These coefficients tell us how these details are linearly related to each other in UT and LT frames. Greater coefficients in the UT frame mean the details have more globally symmetric variations, and lower coefficients in the UT frame mean the details have more asymmetric variations.

The coefficients are calculated in the UT frame from D8 to D13 for the quiet period, 2001.01.05-01.19, and are shown in Table 5.2. The first result in Table 5.2 shows there is a jump between the coefficients of D10 and D11. The average of the coefficients above D10 is over 0.78 while the coefficients from D8 to D10 are averaged at 0.30. D11 to D13 are more linearly related between the four stations than D8 to D10 in the UT frame. The results indicate the details are separated into two parts, the details above D10 and those at and below D10. The details above level 10 are the globally symmetric parts, which come from the symmetric ring current variations. These variations are not in the range of diurnal variations, so they are not affected by the Sq variation and other diurnal variations. The details of D8-D10 are close to diurnal and semi-diurnal variation periods. The local-

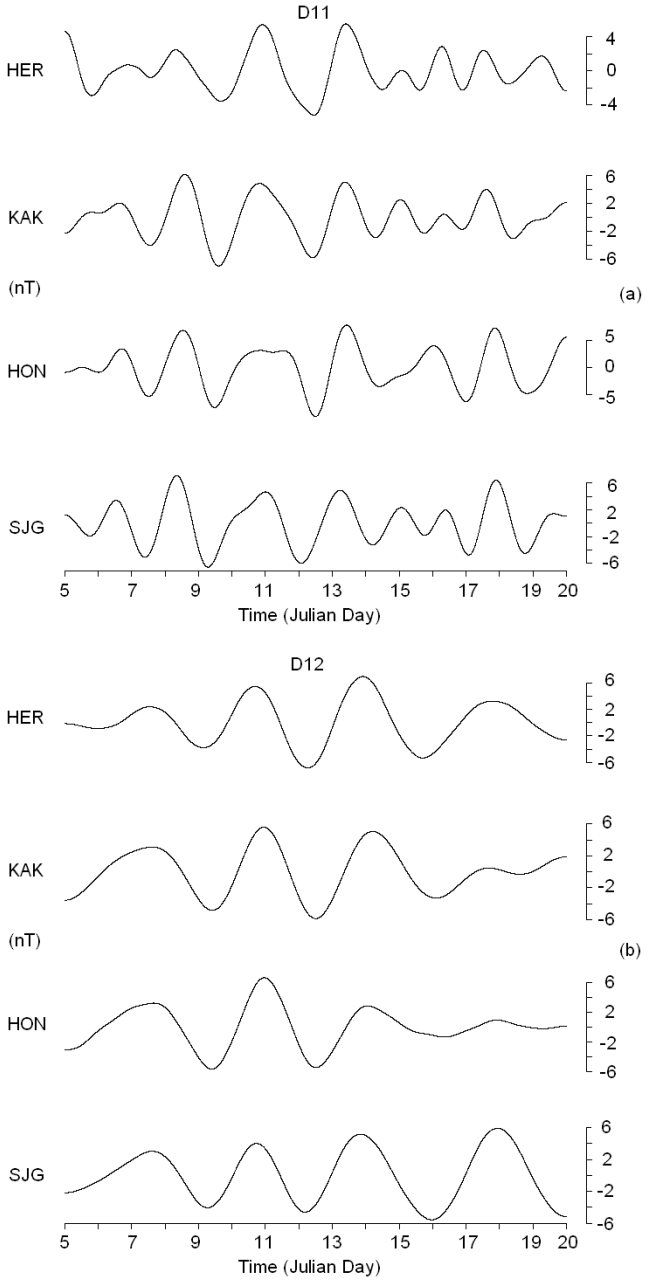


Fig. 5.3. MODWT Details (D11 and D12) for the quiet period during 2001.01.05-01.19 (Julian Day 5-19) in the UT frame.

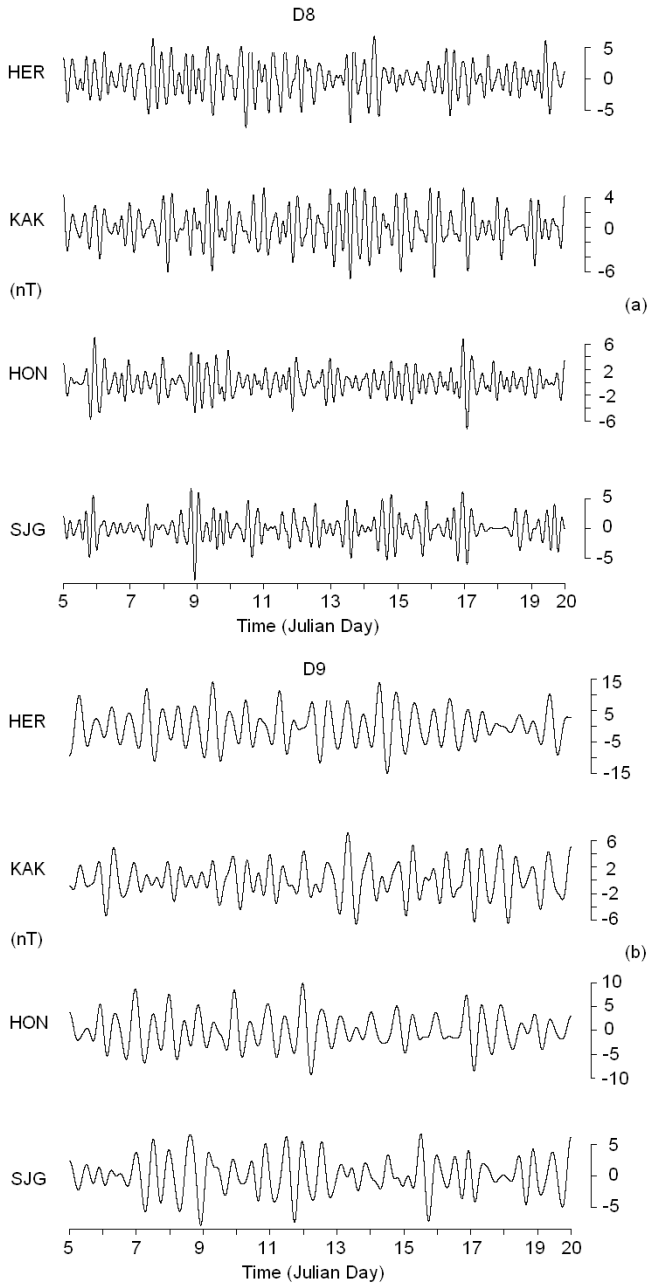


Fig. 5.4. MODWT Details (D8 and D9) for the quiet period during 2001.01.05-01.19 (Julian Day 5-19) in the UT frame.

time dependent components, such as the Sq variation, substorms and the tail current, have significant effects in the variations of D8-D10.

Table 5.2. The correlation coefficients in the UT frame for D8 to D13 for the quiet period during 2001.01.05-01.19.

Coefficients for quiet period (2001.01.05-01.19)

In UT	KAK_SJG	KAK_HON	KAK_HER	SJG_HON	SJG_HER	HON_HER
D8	0.07	0.55	0.52	0.40	0.21	0.33
D9	0.17	0.47	0.43	0.49	-0.15	-0.08
D10	-0.13	0.57	0.05	-0.40	-0.04	-0.40
D11	0.72	0.79	0.72	0.75	0.61	0.62
D12	0.67	0.94	0.75	0.65	0.91	0.69
D13	0.90	0.87	0.92	0.75	0.96	0.84

After comparing the correlation coefficients in the UT frame, the coefficients are calculated in the LT frame from D8 to D13 for the same quiet period (2001.01.05-01.19). Greater coefficients in the LT frame mean that the details are more related to local-time dependent components. The results are shown in Table 5.3. The coefficients above level 10 decrease to averagely 0.56, which further indicate the details above D10 are symmetric in global scale. The coefficients of Detail 13 do not reduce much because D13 is a long-period variation considering the several-hour shift. The more interesting part is the coefficients of D8 to D10 did not clearly increase after the timeframe shifted from UT to LT. The reason is in

diurnal variation, there are both local-time dependent component, such as the effects of the Sq variation, and global symmetric component, such as the effects of the ring current. None of them are dominant in quiet periods. So the coefficients in UT or LT frames are not significantly different in D8-D10.

Table 5.3. The correlation coefficients in the LT frame (SJG as reference) for D8 to D13 for the quiet period during 2001.01.05-01.19.

Coefficients for quiet period (2001.01.05-01.19)

In LT	KAK_SJG	KAK_HON	KAK_HER	SJG_HON	SJG_HER	HON_HER
D8	0.11	-0.36	0.09	0.29	0.18	0.06
D9	0.12	-0.33	-0.01	-0.43	0.36	-0.23
D10	0.18	0.22	0.22	0.55	0.54	0.36
D11	0.50	0.62	0.41	0.79	-0.05	-0.03
D12	0.77	0.89	0.37	0.74	0.13	0.04
D13	0.86	0.92	0.83	0.66	0.76	0.81

Since the comparison of the LT coefficients shows the symmetric and asymmetric components are comparable to each other in D8-D10 and the Sq effect is still there, we feel there is a need to remove the Sq effect and see if there will be any difference in the coefficients. As in the Wavelet Index of Storm Activity(WISA) procedure (Jach et. al., 2006 [28]), the median values at the same minute of the daily curves in D8-D10 during this quiet period are pulled out to combine a quiet-day curve and removed from the original details. Now,

the rest of D8-D10 are the details with the Sq variation removed. Then, the correlation coefficients of these details with the Sq effects removed are calculated and compared with the original ones for both UT and LT frame. As shown in Table 5.4, the coefficients in UT are not obviously increased. Neither are the ones in LT. This indicates during the quiet period, neither the local-time-dependent components nor global-dependent components are dominant. The Sq variation is only a part of the local-time-dependent variations. This result implies using the quiet-day curve to remove the Sq variation is not sufficient to remove the local-time-dependent components in the observations. Since the Dst index uses the quiet-day curve to remove the local-time-dependent components from the observations, the Dst index is not a clean index for describing symmetric ring current.

Table 5.4. The coefficients in the UT frame after the Sq variation is removed from D8 to D10 compared with the original coefficients for the quiet period during 2001.01.05-01.19.

Coefficients with the removal of Sq variation for quiet period (2001.01.05-01.19)						
In UT	KAK_SJG	KAK_HON	KAK_HER	SJG_HON	SJG_HER	HON_HER
D8	0.19	0.52	0.36	0.47	0.32	0.24
D9	0.26	0.46	0.17	0.36	0.15	-0.03
D10	-0.13	0.58	0.07	-0.38	-0.03	-0.29
Original Coefficients						
D8	0.07	0.55	0.52	0.40	0.21	0.33
D9	0.17	0.47	0.43	0.49	-0.15	-0.08
D10	-0.13	0.57	0.05	-0.40	-0.04	-0.40

After using these correlation coefficients to compare which details have more symmetric or asymmetric components, the magnitudes of different level details are compared with each other to study the strengths of different components. The overall average of absolute magnitudes during the quiet period is shown in Table 5.5. The magnitudes of D8 to D10 are at the same level as D11 to D13. Their relative magnitudes are close to each other except that D10 of HON and HER are much stronger than D11-D13. These results also indicate the local-time-dependent or asymmetric component in diurnal variation is comparable to the global symmetric component during quiet periods.

Table 5.5. The averages of absolute magnitudes from D8 to D13 from different stations for the quiet period during 2001.01.05-01.19.

Averages of absolute magnitudes for quiet period (2001.01.05-01.19)						
Station	D8(nT)	D9(nT)	D10(nT)	D11(nT)	D12(nT)	D13(nT)
KAK	1.85	2.00	2.62	2.33	2.36	1.93
SJG	1.53	2.15	3.16	2.71	2.81	1.13
HON	1.43	2.72	7.81	3.26	2.06	1.96
HER	2.00	4.33	7.16	1.90	2.70	1.22

As the conclusion for quiet periods study, the details above D10 are mainly symmetric components coming from the slowly varying symmetric ring current. The details of D8-D10 are related to diurnal variation, which contains some local-time dependent or asymmetric components. The removed-Sq study shows there are still residues of local-time-dependent components after using the quiet-day curve to remove the Sq variation from diurnal vari-

ation. The strengths of symmetric and asymmetric components are comparable to each other as shown by the magnitude study.

Another quiet period, 2001.06.22-07.07, is studied to confirm these conclusion. The results of correlation coefficients study and magnitude study, shown in Table 5.6 and Table 5.7, are consistent with the results from the first quiet period case study.

Table 5.6. The correlation coefficients in the UT frame from D8 to D13 for the quiet period during 2001.06.22-07.07.

Coefficients for quiet period (2001.06.22-07.07)						
In LT	KAK_SJG	KAK_HON	KAK_HER	SJG_HON	SJG_HER	HON_HER
D8	-0.35	0.01	-0.35	0.26	0.66	0.17
D9	0.46	-0.31	0.59	-0.44	0.27	-0.05
D10	-0.09	-0.46	0.32	0.41	-0.76	-0.24
D11	0.62	0.79	0.69	0.61	0.52	0.59
D12	0.75	0.94	0.93	0.82	0.91	0.95
D13	0.92	0.91	0.95	0.85	0.91	0.87

5.3.2. Storm periods study (2001.03.18-04.03 and 2001.10.15-10.30)

As the comparison to quiet periods study, the same analysis is performed on the storm period during 2001.03.18-04.03. The magnetometer data are decomposed into details with the same MODWT method and compared systematically. As shown in Figure 5.5, the details of D11-D12 show similar disturbances in the UT frame. These are the symmetric components of slow variations coming from the symmetric ring current. The details of

Table 5.7. The averages of absolute magnitudes from D8 to D13 from different stations for the quiet period during 2001.06.22-07.07.

Averages of absolute magnitudes for quiet period (2001. 06.22-07.07)						
Station	D8(nT)	D9(nT)	D10(nT)	D11(nT)	D12(nT)	D13(nT)
KAK	2.68	5.02	4.44	2.23	2.38	0.68
SJG	1.77	4.02	4.93	2.56	2.78	1.40
HON	1.52	2.52	5.80	3.03	3.05	1.09
HER	2.41	4.45	6.10	2.13	2.27	0.87

D8-D9 are shown in Figure 5.6 and their features are quite different from those of quiet periods. There are more clearly shifted patterns in Figure 5.6 than those of quiet periods in D9. These are local-time dependent or asymmetric components connected with diurnal variation. The asymmetric patterns are enhanced during storm periods.

After the visual comparison, the correlation coefficients study is applied to these details. The results of the correlation coefficients are shown in Tables 5.8 and 5.9. In Table 5.8 (UT frame), the jump of coefficients between D10 and D11 is as obvious as that of quiet periods study, but the coefficients are greater than those in quiet periods. The average of D8-D10 is around 0.49, while the average of D10-D13 is around 0.98. In Table 5.9 (LT frame), the average of D8-D10 is around 0.25, while the average of D10-D13 is 0.72. The coefficients of both D8-D9 and D11-D13 in UT are greater than those in LT. This indicates not only the slow variations (multiple-day scale) coming from the ring current during storm periods are mainly global symmetric components, but also the variations near daily scale have more symmetric components. The greater coefficients in UT during storm periods indicate the

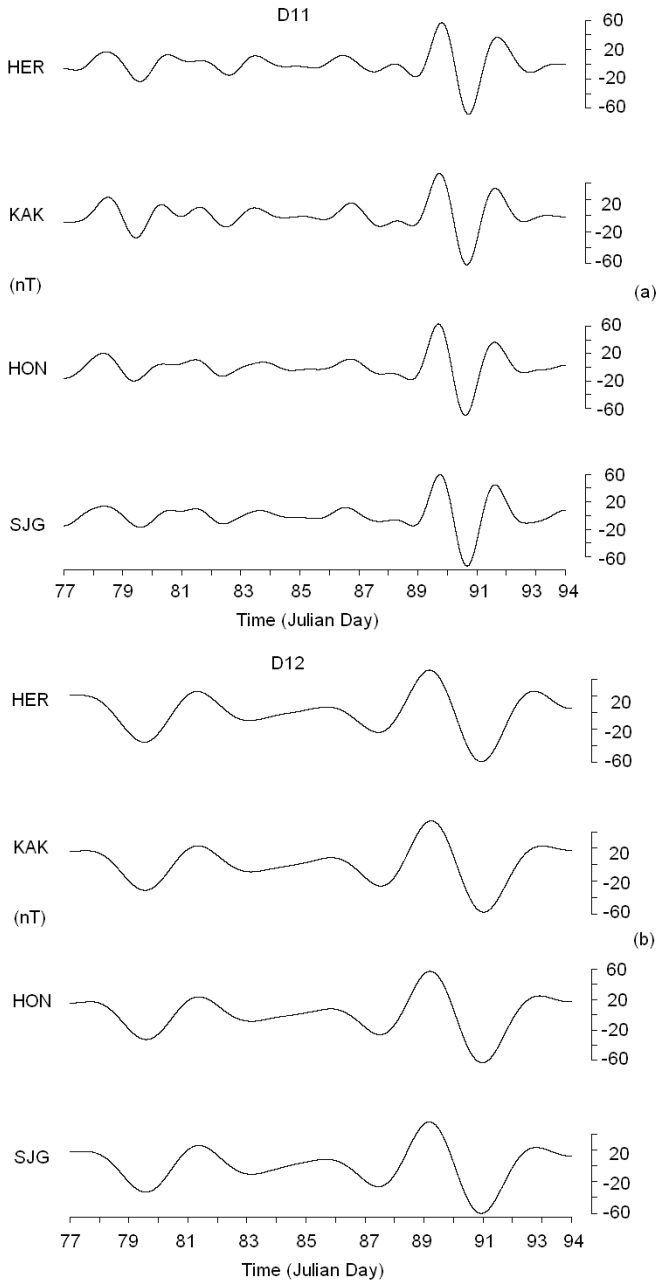


Fig. 5.5. MODWT Details (D11 and D12) for the storm period during 2001.03.18-04.03 (Julian Day 77-93) in the UT frame.

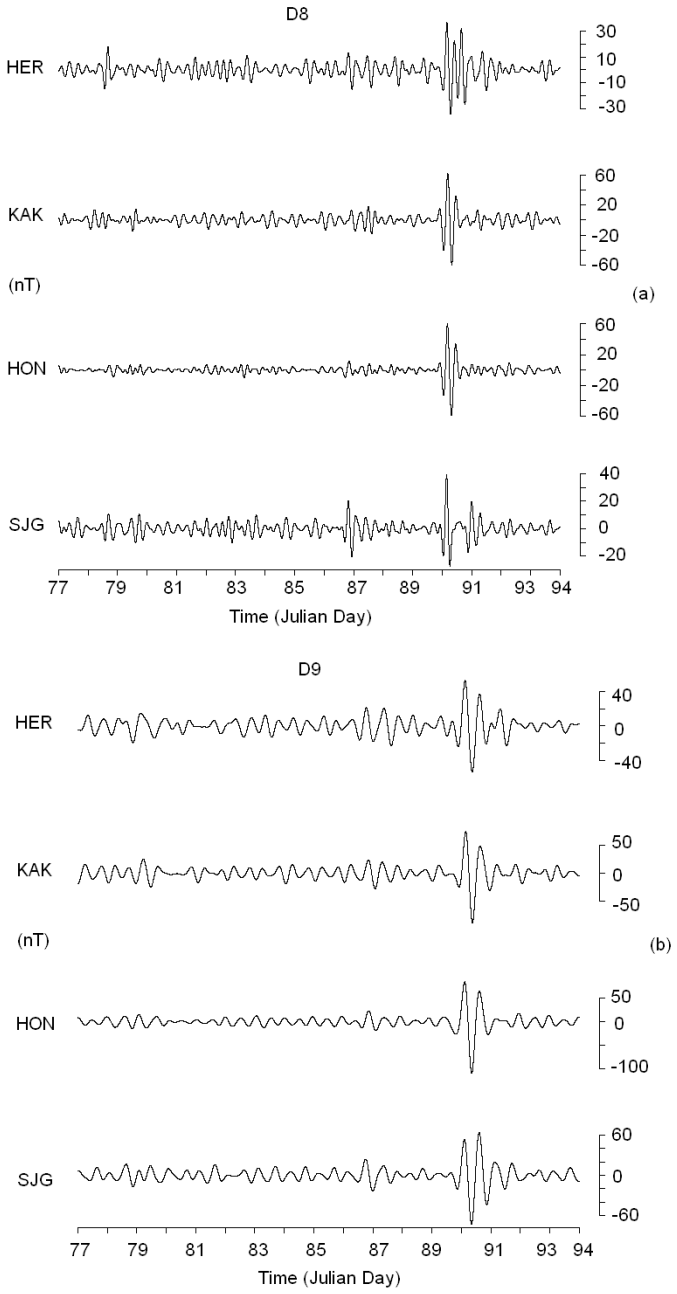


Fig. 5.6. MODWT Details (D8 and D9) for the storm period during 2001.03.18-04.03 (Julian Day 77-93) in the UT frame.

symmetric component increases because of the enhancements of the symmetric ring current during storm periods.

Table 5.8. The coefficients in the UT frame from D8 to D13 for the storm period during 2001.03.18-04.03.

Coefficients for storm period (2001.03.18-04.03)						
In UT	KAK_SJG	KAK_hon	KAK_HER	SJG_HON	SJG_HER	HON_HER
D8	0.12	0.77	0.17	0.46	0.60	0.39
D9	0.58	0.63	0.76	0.70	0.66	0.63
D10	0.60	0.64	0.31	0.45	-0.10	0.22
D11	0.96	0.97	0.95	0.98	0.96	0.92
D12	0.99	1.00	0.98	1.00	1.00	0.99
D13	1.00	1.00	1.00	1.00	1.00	1.00

The correlation coefficients of the details with removed Sq for this storm period in D8, D9, and D10 are also calculated. The results are shown in Table 5.10. Coefficients of D8 and D9 increase about 0.10 and 0.12 after removing the Sq variation from original coefficients, but coefficients of D10 are almost the same as before. The results indicate the Sq variation in D8-D9 is more significant during storm periods than during quiet periods. After removing the Sq variation, the remains of diurnal variation have more symmetric components than these during quiet periods. These are caused by the enhanced ring current.

Since symmetric components exist in both D8-D10 and D11-D13, the magnitude analysis is applied to find out which details have more strength of symmetric components during storm periods. The average magnitudes are shown in Table 5.11. The results are quite different from those of quiet periods. All details are enhanced during the storm period,

Table 5.9. The coefficients in the LT frame from D8 to D13 for the storm period during 2001.03.18-04.03.

Coefficients for storm period (2001.03.18-04.03)						
In LT	KAK_SJG	KAK_HON	KAK_HER	SJG_HON	SJG_HER	HON_HER
D8	-0.05	-0.51	-0.52	0.16	-0.01	0.28
D9	-0.26	-0.06	-0.37	-0.50	-0.04	0.29
D10	-0.42	0.30	0.11	0.43	-0.14	-0.12
D11	0.26	0.90	0.65	0.61	-0.44	0.33
D12	0.82	0.97	0.77	0.93	0.29	0.60
D13	0.94	0.99	0.93	0.96	0.75	0.89

Table 5.10. The coefficients in the UT frame after the Sq variation removed from D8 to D10 comparing with the original coefficients for the storm period during 2001.03.18-04.03.

Coefficients with the removal of Sq variation for storm period (2001.03.18-04.03)						
In UT	KAK_SJG	KAK_HON	KAK_HER	SJG_HON	SJG_HER	HON_HER
D8	0.35	0.82	0.39	0.55	0.54	0.46
D9	0.67	0.89	0.76	0.79	0.80	0.77
D10	0.58	0.64	0.31	0.44	-0.12	0.23
Original Coefficients						
D8	0.12	0.77	0.17	0.46	0.60	0.39
D9	0.58	0.63	0.76	0.70	0.66	0.63
D10	0.60	0.64	0.31	0.45	-0.10	0.22

which means both asymmetric and symmetric components are enhanced during the storm period. The magnitudes of D11-13 count for about 70 percent of the total variations. The symmetric components dominate during the storm and can be pulled out to represent the variations of the symmetric ring current for multiple-day scale study during storm periods. It needs to be mentioned here. The result, which the symmetric components are dominating during storm periods, is the statistical result for the timescale of multiple days. For the shorter timescale, like the main phase of storms, the asymmetric component could be stronger than the symmetric component.

Table 5.11. The averages of absolute magnitudes from D8 to D13 from different stations for the storm period during 2001.03.18-04.03.

Averages of absolute magnitudes for quiet period (2001.03.18-04.03)						
Station	D8(nT)	D9(nT)	D10(nT)	D11(nT)	D12(nT)	D13(nT)
KAK	5.19	9.28	8.07	11.71	17.82	18.29
SJG	3.61	8.05	11.44	12.35	18.55	18.06
HON	3.38	8.59	13.74	12.39	18.62	21.96
HER	4.34	7.26	14.50	12.00	18.00	18.23

Furthermore, another storm period during 2001.10.15-10.30 was also studied. The results in Table 5.12 and Table 5.13 are consistent with those of the period, 2001.03.18-04.03.

5.4. Conclusion and discussion

In order to separate the global symmetric variations in the magnetic disturbances,

Table 5.12. The coefficients in the UT frame from D8 to D13 for the storm period during 2001.10.15-10.30.

Coefficients for storm period (2001.10.15-10.30)						
In UT	KAK_SJG	KAK_HON	KAK_HER	SJG_HON	SJG_HER	HON_HER
D8	0.09	0.33	0.30	0.38	0.38	0.40
D9	0.31	0.10	0.51	0.38	0.39	0.10
D10	0.54	0.58	0.23	0.39	-0.03	0.07
D11	0.86	0.92	0.91	0.93	0.93	0.89
D12	0.96	1.00	0.98	0.97	0.98	0.98
D13	1.00	1.00	1.00	1.00	1.00	1.00

Table 5.13. The average absolute magnitudes from D8 to D13 from different stations for the storm period during 2001.10.15-10.30.

Average absolute magnitudes for storm period (2001.10.15-10.30)						
Station	D8(nT)	D9(nT)	D10(nT)	D11(nT)	D12(nT)	D13(nT)
KAK	3.03	5.83	7.95	7.99	9.84	15.79
SJG	2.62	4.44	9.13	8.17	9.68	16.96
HON	2.59	5.03	12.25	8.11	10.05	17.92
HER	3.01	4.70	10.15	8.07	10.61	17.70

which reflect the variations of the symmetric ring current, from the asymmetric variations caused by local-time dependent or asymmetric components, such as the Sq variation, the tail current and other currents, the MODWT method is used to study the wavelet spectra of the H component of geomagnetic observations. After the H component is decomposed into different time series, the MODWT details, which represent different variations on different timescales, visual comparison study, wavelet cross-spectrum analysis, and magnitude comparison study are performed to investigate the characteristics of symmetric and asymmetric components on various timescales for both quiet and storm periods. The results are summarized as follows:

a. The slow-time-varying components of the ring currents are largely globally symmetric as indicated by the visual comparison study of the wavelet details and the wavelet cross-spectrum analysis. For both quiet and storm times, there are in-phase variations in details above level 11, which are connected to variations of multiple-day timescale, shown by the data of all Dst stations. The wavelet cross spectrum correlation study shows these slow time-varying components have a highly linear relationship between these stations for both quiet and storm periods in the UT frame. During storm periods, these components are more globally symmetric than those during quiet periods, due to the enhancement of the symmetric ring current. The visual comparison study and the wavelet cross spectrum analysis also show that significant asymmetric or local-time dependent components exist in the details of diurnal timescales. They are also enhanced during storm times due to the enhancements of the asymmetric current sources, such as partial ring current and tail current.

b. The magnetic effect of the symmetric components is comparable to the effect of the asymmetric (or local-time-dependent) components during quiet periods, but dominates during storm periods. The magnitude study shows the strength of the symmetric components counts for about 40% of all variations during quiet periods, but over 70% during storm periods. During storm periods, the magnetic disturbances associated with both the symmetric and asymmetric parts of the ring currents increase significantly, but the increase of the symmetric ring current is much larger than that of the asymmetric current and it

becomes dominant. This result is based on the statistical study of multiple-day timescale variations. For shorter timescales, such as the main phase of storms, the asymmetric component could be stronger than the symmetric component.

c. The comparison of cross correlations between original and Sq-removed details shows using the quiet-day curve is not sufficient to remove the asymmetric (or local-time-dependent) components from the observations. Since the Dst index uses the quiet-day curve to remove the Sq variation, the Dst index is not a clean index to describe the variations of the symmetric ring current.

All these results present a statistical and quantitive picture of the symmetric and asymmetric variations in the geomagnetic H component spectrum. The details above level 11 are globally symmetric variations and can be used to investigate the large timescale variations of the symmetric ring current, especially during storm periods. For future work, the wavelet analysis can be applied to mid- and high-latitude stations to reconstruct the variations of the symmetric ring current. When the method is also applied to the Z component, the reconstructions of symmetric variations in H and Z components can be used to investigate the spatial and temporal variations of the symmetric ring current.

CHAPTER 6
SPATIAL VARIABILITY OF THE RING CURRENT DURING STORM AND QUIET PERIODS

In the previous chapter, we find the details above D10 of the magnetic disturbances mainly come from the symmetric components of the ring current and the details from D8 to D10 have significant effects of the asymmetric components of the ring current. In the following study, we will use the details above D10 to reconstruct the disturbances of the geomagnetic fields that are caused by the symmetric components of the ring current. These reconstructed magnetic field disturbances are then used to study the spatial and temporal variations of the symmetric ring currents, once we set up the suitable mathematical schemes that can derive the variations of symmetric ring current from the geomagnetic field disturbances in terms of electromagnetic physical principles.

The study of the ring current has been one of the most important subjects for magnetospheric physics since the early time of space science. The concept of the ring current was started with the pioneer work done by Carl Stoermer [42], [43], [44], and then followed by Adolf Schmidt, who suggested the development of a ring current was the cause of the main phase of magnetic storms [45]. Chapman and Ferraro contributed their theoretical and experiment work, which established the location of and driving force for this current system [46], [47], [48]. The study of the ring current was further pursued by Akasofu, Alfven, Dessler, Parker, Singer, Smith, and others [9], [49], [50], [51], [52], [53]. Significant studies of the ring current were performed by using satellites experiments. The ring current models have been connected to the magnetosphere and ionosphere Models with the inputs of the Interplanetary Magnetic Field (IMF) and Solar Wind parameters, which are obtained from in situ measurements of satellite observations, such as Polar, ACE, Wind, Image and so on. The comparisons among various models are carried out widely [3], [10], [27], [54], [55], [56], [57]. For an example, Burton, McPherron and Russell

developed an algorithm that is used to predict the ground-based Dst index based on the velocity and density of the solar wind and the north-south solar magnetospheric component of the interplanetary magnetic field. The three key elements of this model are a parameter based on the solar wind dynamic pressure, an injection rate linearly proportional to the dawn-to-dusk component of the interplanetary electric field, and an exponential decay rate of the ring current with an e folding time of 7.7 hours [54].

Comparing the research of the ring current with the measurements of satellite observations, the study of the ring current with ground-based measurements are less investigated [34], [35], [58], [59], [60]. In this chapter, we used the wavelet filtered geomagnetic field records to study the variations of the ring current in spatial and temporal domains. The main focus is on the radius variability of the symmetric ring current during storm and quiet periods. First, we decompose the complex variations of the symmetric ring current into four simple situations and the complex variations can then be the combinations of these four situations if the time interval is fine enough such as thirty or sixty minutes. By using the multiple components of geomagnetic field data from multiple locations, we can separate four simplified situations based on the physics criteria. Then the data can be processed using different mathematical schemes to calculate the spatial and intensity variations of the symmetric ring current accordingly. Actually, in this dissertation research, the focus is to study the radius (R) variability of the symmetric ring current during the storm and quiet periods. For more complicated variations of the ring current, a mathematical scheme is proposed in which the combined variability of the radius and intensity of the symmetric ring current can be studied by using an iterative algorithm.

6.1. Mathematical scheme for the study of the symmetric ring current

The symmetric ring current can be simplified as a simple wire current at the geomagnetic equator plane of the dipole geomagnetic field model (Figure 6.1). The dipole model of the Earth's geomagnetic field is a first order approximation of the complex Earth's magnetic field (Figure 6.2).

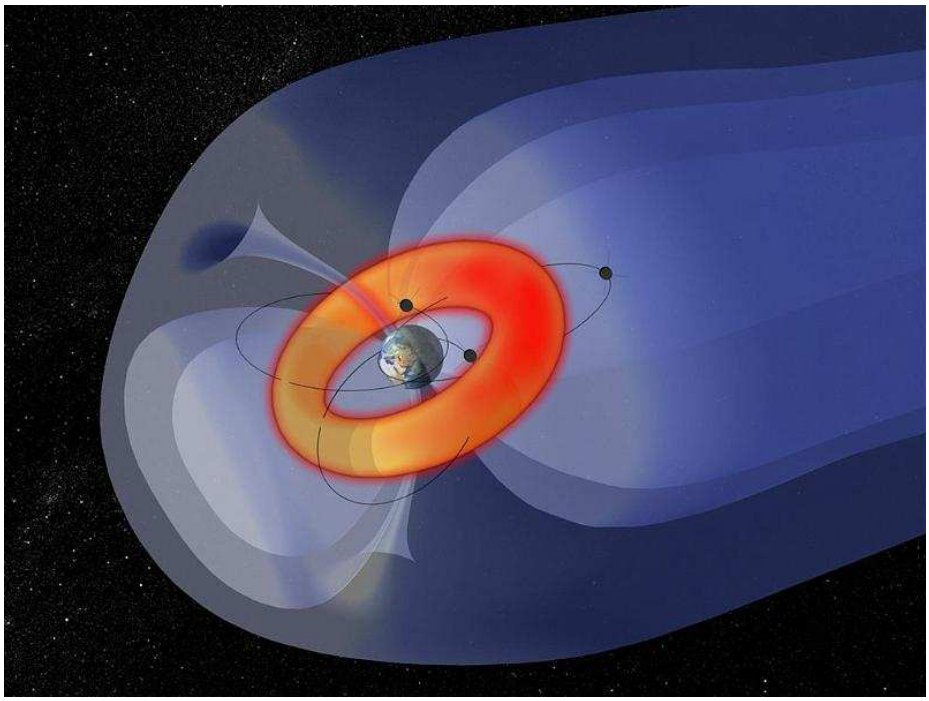


Fig. 6.1. Artist's rendition of the symmetric ring current over the Earth's magnetic equatorial region.

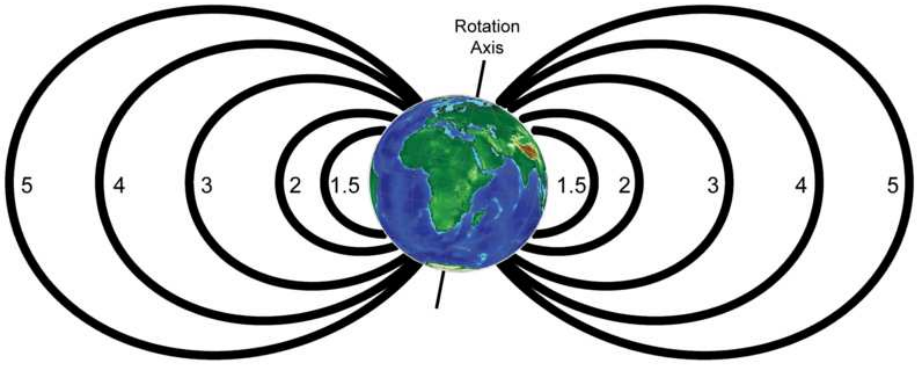


Fig. 6.2. The dipole field model of Earth's magnetic field by the courtesy of Dr. Daniel I Golden.

By applying the Biot-Savart Law, we can calculate the magnetic field generated by the current with the following formula:

$$\vec{B} = \int \frac{\mu_0}{4\pi} \frac{I d\vec{l} \times \hat{r}}{|r|^2} \ , \tag{6.1}$$

where I is the current, $d\vec{l}$ is a vector whose magnitude is the length of the differential element of the wire, and whose direction is the direction of the current, $\vec{B}$ is the net magnetic field, μ_0 is the magnetic constant, vacuum permeability, $\hat{r}$ is the displacement unit vector in the direction pointing from the wire element towards the point at which the field is being computed, and $\vec{r} = r\hat{r}$ is the full displacement vector from the wire element to the point at which the field is being computed.

The magnetic field generated by the ring current has the horizontal component B_H and vertical component B_Z as follows:

$$B_H = \frac{(r^2 - 2R^2)R^2 I sin\theta \mu_0}{4(r^2 + R^2)^{5/2}} \ , \ and \tag{6.2}$$

$$B_Z = \frac{(2r^2 + 2R^2)R^2 I cos\theta \mu_0}{4(r^2 + R^2)^{5/2}} \ , \tag{6.3}$$

where r is the Earth radius, R is the ring current radius, I is the intensity of the ring current, θ is the co-geomagnetic-latitude from 0-180 degree, μ_0 and is vacuum permeability.

We need to note from Equation 6.1 to 6.2 and 6.3, an approximation is made by assuming the radius of the symmetric ring current is not too close to the Earth's center. The details are as follows.

Magnetic field vector potential A is:

$$A_\theta(r, \theta) = \frac{\mu_0 I R^2}{4\pi} \int_0^{2\pi} \frac{cos\phi' \, d\phi'}{\sqrt{R^2 + r^2 - 2Rrsin(\theta)cos(\phi')}} \ , \tag{6.4}$$

where R is the radius of the symmetric ring current to the center of the Earth, r is the radius of the Earth, θ is the magnetic co-latitude angle, and ϕ' is the magnetic longitude angle.

If we manipulate the parts inside the integral, we can have

$$A_\theta(r,\theta) = \frac{\mu_0 I R^2}{4\pi(R^2+r^2)} \int_0^{2\pi} \frac{cos(\phi^{'})d\phi^{'}}{\sqrt{1-\frac{2Rrsin(\theta)cos(\phi^{'})}{R^2+r^2}}} \ . \tag{6.5}$$

For the following part in the square root in the denominator,

$$\sqrt{1-\frac{2Rrsin(\theta)cos(\phi^{'})}{R^2+r^2}} \ . \tag{6.6}$$

If this part is close to zero, which is

$$\frac{2Rrsin(\theta)cos(\phi^{'})}{R^2+r^2} \ , \tag{6.7}$$

and by the Taylor Series,

$$(1+x)^m = 1 + mx + \frac{m(m-1)x^2}{2!} + \cdots , \tag{6.8}$$

we have

$$\sqrt{1-\frac{2Rrsin(\theta)cos(\phi^{'})}{R^2+r^2}} = \tag{6.9}$$
$$1 + (-\frac{1}{2})(\frac{-2Rrsin(\theta)cos(\phi^{'})}{R^2+r^2}) + (\frac{(-\frac{1}{2})(-\frac{1}{2}-1)}{2\times 1})(\frac{-2Rrsin(\theta)cos(\phi^{'})}{R^2+r^2})^2 + \cdots .$$

So, in this case, we can take an approximation as

$$\sqrt{1-\frac{2Rrsin(\theta)cos(\phi^{'})}{R^2+r^2}} = 1 + \frac{Rrsin(\theta)cos(\phi^{'})}{R^2+r^2} + \frac{3}{8}\frac{R^2r^2sin^2(\theta)cos^2(\phi^{'})}{(R^2+r^2)^2} + \cdots . \tag{6.10}$$

To make this approximation valid, we need to keep in mind the following conditions are satisfied:

$$R^2 + r^2 >> 2rRsin(\theta)cos(\phi^{'}) \ . \tag{6.11}$$

Then there are either of the following conditions needing to be satisfied:

a. $sin(\theta) \approx 0$.

b. $r \gg R$.

c. $R \gg r$.

d. $cos(\phi') \approx 0$.

It requires the radius of the symmetric ring current should be greater than the radius of the Earth, if we drop the second order terms from the equations. Finally we have Equation 6.2 and 6.3 as the horizontal and vertical component of the magnetic field generated by the symmetric ring current on the surface of the Earth.

We ran a test on the difference between keeping the 2nd order and 1st order terms in the equations by substituting different R, the radius of the ring currents as a ratio to the radius of the Earth, into the magnetic vector potential equations and calculated the difference and relative difference. The results are shown in Figure 6.3. When the radius of the ring current is greater than 4 Re (the radius of the Earth), the relative difference is less than ten percent. Since the ring currents stay between 4 - 8 Re for most cases in both storm and quiet periods, the approximation will be valid.

6.2. Four simplified configurations

The variations of the symmetric ring currents in real world are extremely complicated, but we can always decompose them into four basic configurations, which are as follows:

Configuration 1, Intensity: The ring currents only vary in intensity and stay stationary in the same positions.

Configuration 2, Radius: The ring currents only vary in radius towards or away from the axis of the dipole field.

Configuration 3, Shifted: The ring currents only shift up or down along the dipole field axis and vertically to the equatorial plane.

Configuration 4, Tilted: The ring currents only tilt according to the dipole field axis.

We can consider the complicated variations of the ring current configurations as the combination of these four simple configurations. For example, a typical case of the symmet-

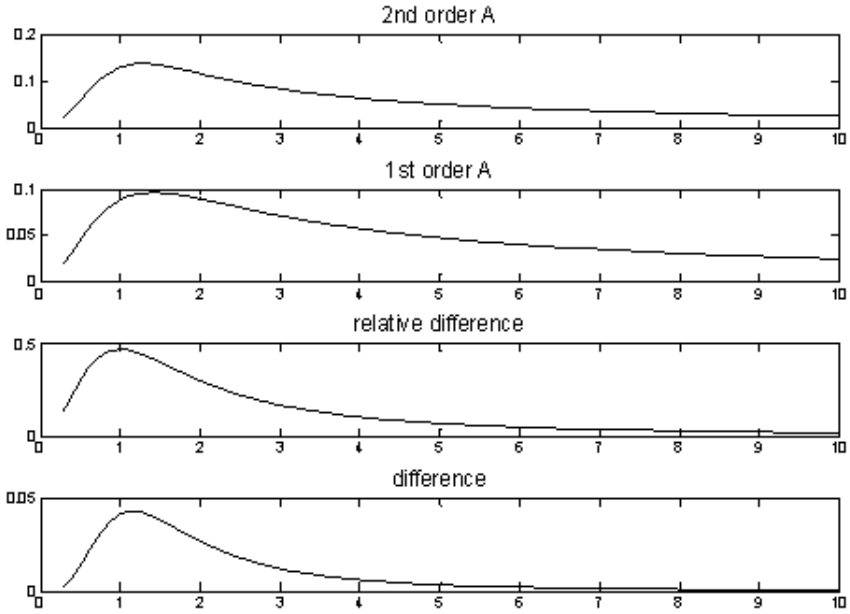


Fig. 6.3. The differences between keeping 2nd and 1st order terms in the vector potentials.

ric ring current variations is the ring current is moving towards the Earth. So the radius of the ring current is changing while the intensity of the ring current is increasing at the same time. But, if we take the time interval that is sufficiently fine, say thirty or sixty minutes, we can consider the variations of the symmetric ring current are only in radius or intensity. The variation becomes that the ring currents shrink for one moment, then the intensity of the ring current increases. The combination can be separated into step-by-step changes.

For each one of these four simple configurations listed above, now we look for the criteria, which can identify the dominant variations during a specific time interval. We assume that initially the ring currents are symmetrical and stationary at the geomagnetic equatorial plane that is defined in terms of the centered and tilted dipole model of the Earth's geomagnetic field. Then magnetic field generated by the ring currents should be symmetric in Z component, which is vertical to the equatorial plane. Since it is axial symmetric, the longitudinal effects are the same and only the latitudinal effects need to be taken into consideration. Supposedly, a magnetometer is placed at the geomagnetic

latitude of *theta*, then the observed changes of magnetic field data include both horizontal and vertical components. The data from multiple locations need to be used. If we apply the criteria in the following to the data, then we can find the dominant configuration during the small time interval.

The first criterion is to check two specific ratios, which are the ratios of the horizontal component changes over the vertical component changes of the geomagnetic data from station one and station two at the same latitudes, but at different longitudes.

$$\frac{\triangle B_{H1}}{\triangle B_{Z1}} = \frac{\triangle B_{H2}}{\triangle B_{Z2}} \ , \tag{6.12}$$

where station one and station two are from same latitude but different longitude. If both sides in the equation are not equal, then the configuration is the tilted configuration. If they are equal, then we need to go to the second criterion. The reason is the tilted configuration is the only configuration that is not symmetric in longitude among these four configurations in terms of Equation 6.2 and 6.3. The other three configurations are all symmetric in longitudinal effects.

The second criterion is to check another two ratios, which are the ratios of the horizontal component changes over vertical component changes of the geomagnetic data from station one and station two at the same longitudes, but at different latitudes.

$$\frac{\triangle B_{H1}}{\triangle B_{Z1}} = \frac{\triangle B_{H2}}{\triangle B_{Z2}} \ , \tag{6.13}$$

where the changes of station one and station two are from two stations at the same longitude, but different latitudes. If both sides are not equal, then the configuration is the shifted configuration. If they are equal, then we need to go to the third criterion. The reason is in the shifted configuration, the magnetic disturbance is latitude dependent and the ratios calculated by Equation 6.2 and 6.3 vary for different magnetic latitudes. In contrast, these ratios do not vary in terms of magnetic latitudes in the radius and intensity configurations.

The third criterion is to check the two ratios that are the ratios of the horizontal

component changes over the vertical component changes of the geomagnetic data from the same station for two continuous time intervals.

$$\frac{\triangle B_{H_{t1}}}{\triangle B_{Z_{t1}}} = \frac{\triangle B_{H_{t2}}}{\triangle B_{Z_{t2}}} \ , \tag{6.14}$$

where the changes are from same station, but different time intervals. If both sides are not equal, then the configuration is the radius configuration. If they are equal, then the configuration is the intensity. The reason is in the intensity configuration, the ratio of the changes of H component over the changes of Z component keeps the same value, which should be tangent of the co-latitude by Equation 6.2 and 6.3. In contrast, this ratio will change for the radius configuration.

6.3. Study of the radius variations of the symmetric ring current

Deriving the complete information of spatial and temporal variations of the ring current by using the ground-based magnetometer data or studying the combined effects of the simplified four configurations of the ring current variations is a huge task. In this research effort, we will focus on the study of the radius variations of the symmetric ring current. The mathematical scheme is described in the following.

First, we extract the magnetic disturbances for two time intervals of the geomagnetic record from one station, which have been processed by the wavelet process mentioned in the previous chapter, and reconstruct them for the study of geomagnetic effects caused by the symmetric ring current variations.

Second, we use the following working equations to calculate the ring current radius variations by using the variations of both horizontal and vertical components. For a small interval, say sixty minutes, the variations can be close to the deferential changes.

$$\frac{\triangle B_H}{\triangle B_Z} \approx \frac{dB_H}{dBZ} = \frac{\frac{dB_H}{dR}}{\frac{dB_Z}{dR}} = \frac{2R^5 - 11R^3r^2 + 2Rr^4}{-2R^5 + 2R^3r^2 + 4Rr^4} \frac{sin\theta}{cos\theta} \ . \tag{6.15}$$

By using this equation, we can calculate the radius variations of the ring current based on the geomagnetic field variations between two time intervals.

After the criteria and the working equations for calculating the variations of the symmetric ring currents for the radius variations, we can use the geomagnetic records from multiple stations to study the spatial (radius) variations of the symmetric ring currents during both storm and quiet periods.

As described in the previous chapter, the temporal and spatial variability of the symmetric ring current can be separated into different categories based on the relationships between multiple components of the magnetic field from multiple stations. The wavelet analysis is applied to the geomagnetic data to indentify the details associated with symmetric ring current. Then these details are reconstructed for studying the variability of symmetric ring current. The variations of the symmetric ring current can be quantitatively studied by using reconstructed geomagnetic data and current-magnetic effect inversion schemes. Specifically, in this research effort, the spatial variability of the symmetric ring current for years 2001 and 2002 is systematically studied for various seasonal and geomagnetic conditions.

First, the geomagnetic data are processed by the wavelet procedures introduced in Chapters 4 and 5. The original data are decomposed into different details with different time-scale variations. The details above level ten are used to reconstruct effects generated by the symmetric ring currents variations. The time resolution of original data is one minute. In order to get rid of the high-frequency noises, the original data are smoothed by 30 minutes and prepared as an input for the criterion of the radius configuration.

Second, the filtered and smoothed data are checked in terms of the criterion of the radius configuration. The radius criterion is used to check two ratios, which are the ratios of the horizontal component changes over the vertical component changes of the geomagnetic data from the same station for two continuous time intervals. If they are not equal, then the configuration is the radius configuration. The period will be marked as a radius configuration period.

Third, after the period of radius variation has been identified and selected, the geomagnetic data from multiple stations are then processed by wavelet analysis and reconstructed to study the radius variations of the symmetric ring current. There are about 20 cases in 2001 and 2002 for both storm and quiet periods. The magnetic components of both H and Z are used in the calculation. The sample results are shown in Figures 6.4 and 6.5.

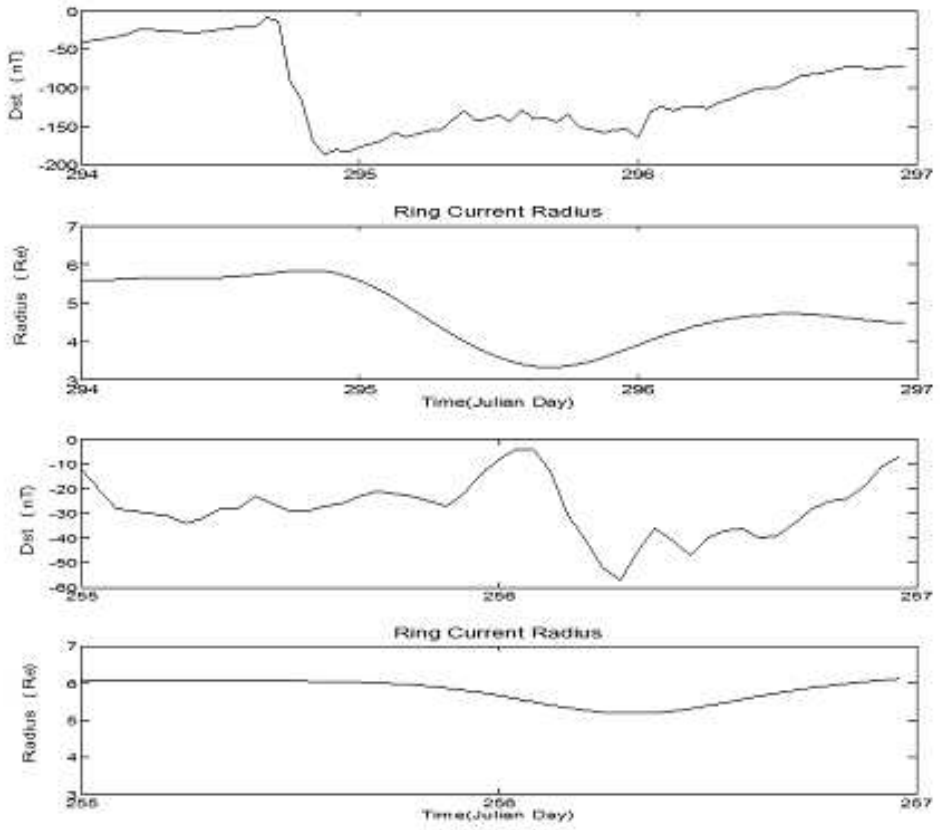


Fig. 6.4. The radius variations of the symmetric ring current in 2001 for quiet (upper figure) and storm (lower figure) periods.

In Figure 6.4, the two cases in 2001 are shown. One is during a storm period and the other is during a quiet period. In order to compare the radius variations of the symmetric ring current to the geomagnetic disturbances, the Dst indices are shown in the figures too. In Figure 6.4, for the storm period from Julian day 294 to 296, a strong storm lasted for over 30 hours. Before the storm began, the symmetric ring current was at about 5.6 Re

(the radius of the Earth). After the Dst index reached a minimum value of about negative 200nT, the radius of the symmetric ring current started to decrease during the main phase of the strong storm on Julian Day 295, and reached the smallest radius, which was about 3.3 Re, on Julian Day 296. There is a delay between the minimum of the storm main phase and the radius minimum of the symmetric ring current. The delay should be due to the reason the asymmetric ring current is mostly enhanced during the main phase, and the symmetric ring current is dominant after that. Then during the recovery phase, the symmetric ring current moved away from the Earth from 3.3 Re to 4.5 Re. For the quiet period case, the radius of the symmetric ring current stayed at about 6 Re until the small disturbance (-60 nT in the Dst Index) happened on Julian Day 266. The radius moved towards the Earth (5.2 Re) slightly during the disturbance, then moved away from the Earth, and back to the location before the disturbance (6 Re).

In Figure 6.5, the upper case shows the radius variations of the symmetric ring current during a quiet period from Julian Day 40 to 42 in 2002. The result is similar to the case during a quiet period in 2001. The symmetric ring current stayed at about 6 Re away from the Earth. When the disturbances happened, the radius changed from 6 Re to 5.6 Re, then back to 6 Re. For the case during the storm period, there was actually one strong disturbance (-200nT) and one medium disturbance (-80nT) from Julian Day 250 to 255. The radius of the symmetric ring current decreased from 5.6 Re to 3.5 Re. Then during the recover phase, the radius increased from 3.5 Re to 5.1 Re. When the second mild disturbance happened, the ring current moved inwards again and moved back to 5 Re after the disturbance.

The other cases in 2001 and 2002 show consistent results. For quiet periods, the radius of the ring current is at about 6 Re. For strong storm periods, the radius varies from 6 Re to 3 Re. This is consistent with results from study of the ring current using the satellite in situ observations [21].

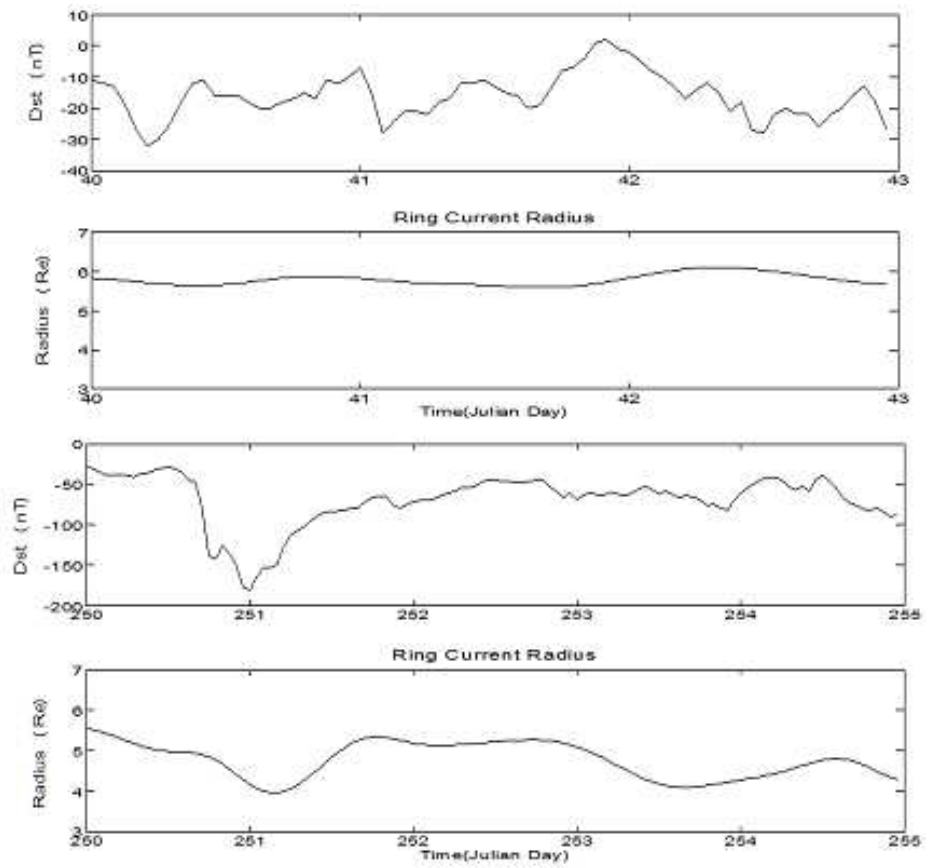


Fig. 6.5. The radius variations of the symmetric ring current in 2002 for quiet (upper figure) and storm (lower figure) periods.

6.4. Discussion and future work

We studied the radius variations of the symmetric ring current by using the ground-based magnetometer data and showed sample results for storm and quiet periods in 2001 and 2002 in the previous section.

The results are consistent with the satellite measurements, which show during the quiet periods, the symmetric ring current basically stays at about 6 Re from the Earth and during the storm periods, the symmetric ring current starts to move towards the Earth during the main phase, and moves away from the Earth during the recovering phase. The range of the radius variations are from 3-6 Re depending on the magnitude of the geomagnetic disturbances. For a strong geomagnetic storm, the symmetric ring current could be pushed

towards the Earth to 3 Re. For a weak storm, the radius variations from 6 Re to 5 Re. There is a delay between the minimum of the storm main phase and the radius minimum of the symmetric ring current. The reasonable explanation is during the main phase of the geomagnetic storm, the asymmetric ring current is the most enhanced part. The calculation in this research is focused on the symmetric ring current variations. The symmetric ring current dominates more after the main phase peak. During the recovery phase, the symmetric ring current and the Dst index are almost in the same phase.

As we mentioned in the previous section of this chapter, the variations of the symmetric ring current are much more complicated than just radius variations. A realistic approach will be combining the four simple configurations with each other. For example, the ring current is moving towards the Earth while its intensity is increasing. We did some exploratory work on those configurations. A possible solution for the R-I variation combination is given as follows:

From the Biot-Savart Law (Equation 6.1), the magnetic field generated by the ring current has horizontal component BH and vertical component BZ as in Equations 6.2 and 6.3.

$$B_H = \frac{(r^2 - 2R^2)R^2 I sin\theta\mu_0}{4(r^2 + R^2)^{\frac{5}{2}}},$$

$$B_Z = \frac{(2r^2 + 2R^2)R^2 I cos\theta\mu_0}{4(r^2 + R^2)^{\frac{5}{2}}},$$

where r is the Earth's radius, R is the ring current radius, I is the intensity of the ring current, θ is the co-geomagnetic latitude from 0-180 degree, and μ_0 is vacuum permeability.

If R changes from R_0 to $R_0 + \Delta R$ while I changes from I_0 to $I_0 + \Delta I$ for the horizontal component part,

$$B_H(R_0 + \Delta R, I_0 + \Delta I) = \frac{(r^2 - 2(R_0 + \Delta R)^2)(R_0 + \Delta R)^2(I_0 + \Delta I)sin\theta\mu_0}{4(r^2 + (R_0 + \Delta R)^2)^{5/2}} \ . \qquad (6.16)$$

Expanding,

$$B_H(R_0+\Delta R, I_0+\Delta I) = \frac{(r^2-2(\Delta R)^2-2(R_0)^2-4R_0\Delta R)((\Delta R)^2+(R_0)^2+2R_0\Delta R)(I_0+\Delta I)sin\theta\mu_0}{4(r^2+(R_0+\Delta R)^2)^{5/2}} . \tag{6.17}$$

Drop the second order terms in the numerator,

$$B_H(R_0+\Delta R, I_0+\Delta I) = \frac{(r^2-2(R_0)^2-4R_0\Delta R)((R_0)^2+2R_0\Delta R)(I_0+\Delta I)sin\theta\mu_0}{4(r^2+(R_0+\Delta R)^2)^{5/2}} . \tag{6.18}$$

Then,

$$B_H(R_0+\Delta R, I_0+\Delta I) = \frac{(r^2-2(R_0)^2)(R_0)^2I_0sin\theta\mu_0+(r^2-2(R_0)^2)(R_0)^2\Delta Isin\theta\mu_0+(2r^2R_0-8R_0^3)I_0\Delta Rsin\theta\mu_0}{4(r^2+(R_0+\Delta R)^2)^{5/2}}. \tag{6.19}$$

For the denominator part,

$$f(R_0) = (r^2+(R_0)^2)^{5/2} , \tag{6.20}$$

and

$$f(R_0+\Delta R) = (r^2+(R_0+\Delta R)^2)^{5/2} . \tag{6.21}$$

By using the series expansion,

$$f(R_0+\Delta R) = (r^2+(R_0+\Delta R)^2)^{5/2} = f(R_0)+\frac{df}{dR}\Delta R+\frac{1}{2}\frac{d^2f}{dR^2}(\Delta R)^2 . \tag{6.22}$$

Dropping the second order terms, it becomes

$$f(R_0+\Delta R) = (r^2+(R_0)^2)^{5/2}+\frac{2}{5}(r^2+(R_0)^2)^{3/2}\Delta R . \tag{6.23}$$

So if we can neglect the following term

$$f(R_0 + \Delta R) - f(R_0) = \frac{2}{5}(r^2 + (R_0)^2)^{3/2}\Delta R \ , \tag{6.24}$$

which means

$$(r^2 + (R_0)^2)^{5/2} \gg \frac{2}{5}(r^2 + (R_0)^2)^{3/2}\Delta R \ , \tag{6.25}$$

$$r^2 + (R_0)^5 \gg 5R\Delta R \ . \tag{6.26}$$

For ring current variations, $\Delta R \approx \frac{1}{2}Re$ per hour, $r = Re$, $R = (3Re, 7Re)$.

When $R = 3Re$, we have

$$10(Re)^2 > 7.5(Re)^2 \ . \tag{6.27}$$

When $R = 7Re$, we have

$$50(Re)^2 > 17.5(Re)^2 \ . \tag{6.28}$$

So the denominator is close to $4(r^2 + (R_0 + \Delta R)^2)^{5/2}$.

Now, if we define the following:

$$B_{H0}(R_0, I_0) = \frac{(r^2 - 2(R_0)^2)(R_0)^2 I_0 sin\theta\mu_0}{4(r^2 + (R_0)^2)^{5/2}} \ , \tag{6.29}$$

$$\Delta B_{HI}(R_0, I_0 + \Delta I) = \frac{(r^2 - 2(R_0)^2)(R_0)^2 \Delta I sin\theta\mu_0}{4(r^2 + (R_0)^2)^{5/2}} \ , \ and \tag{6.30}$$

$$\Delta B_{HR}(R_0 + \Delta R, I_0) = \frac{(2r^2 R_0 - 8(R_0)^3) I_0 \Delta R sin\theta\mu_0}{4(r^2 + (R_0)^2)^{5/2}} \ . \tag{6.31}$$

Then, for the horizontal component, we have

$$B_H(R_0 + \Delta R, I_0 + \Delta I) = \Delta B_{HI}(R_0, I_0 + \Delta I) + \Delta B_{HR}(R_0 + \Delta R, I_0) + B_{H0}(R_0, I_0) \ . \tag{6.32}$$

For the vertical component, we have the similar result, as follows:

$$B_{Z0}(R_0, I_0) = \frac{(2r^2 + 2(R_0)^2)(R_0)^2 I_0 cos\theta\mu_0}{4(r^2 + (R_0)^2)^{5/2}} \ , \tag{6.33}$$

$$\Delta B_{ZI}(R_0, I_0 + \Delta I) = \frac{(2r^2 + 2(R_0)^2)(R_0)^2 \Delta I cos\theta\mu_0}{4(r^2 + (R_0)^2)^{5/2}} \ , \ and \tag{6.34}$$

$$\Delta B_{ZR}(R_0 + \Delta R, I_0) = \frac{(4r^2 R_0 + 8(R_0)^3) I_0 \Delta R cos\theta\mu_0}{4(r^2 + (R_0)^2)^{5/2}} \ . \tag{6.35}$$

Then, we have

$$B_Z(R_0 + \Delta R, I_0 + \Delta I) = \Delta B_{ZI}(R_0, I_0 + \Delta I) + \Delta B_{ZR}(R_0 + \Delta R, I_0) + B_{Z0}(R_0, I_0) \ . \tag{6.36}$$

Equation 6.32 and 6.36 are linearized equations, where ΔR and ΔI are variables.

For solving these variables, we need initial conditions for I_0 and R_0. The initial conditions can be either from previous R-I variations or satellite data. Future work could be carried on as a follow-on study of this dissertation.

CHAPTER 7
SUMMARY AND DISCUSSION

In the magnetosphere and ionosphere, there are complicated current systems, including the ring current, tail current, field-aligned current, and various electrojets. These currents vary on a wide range of spatial and temporal scales and physically couple with each other. To study the complicated behaviors of these coupled current systems, ground-based magnetometers have been a useful tool, but the recorded magnetometer data are always multi-scaled and intermittent due to the nature of these current systems. To distinguish these geomagnetic effects with multiple temporal and frequency scales, the wavelet analysis technique is especially suitable because of its special abilities of presenting information in both temporal and frequency domains. In this dissertation, the geomagnetic disturbance on the surface of the Earth and the ring current variability are studied by using wavelet analysis and ground-based magnetic data from multiple stations.

First, the strengths of the wavelet analysis over other conventional time-series analyses are explored by systematically comparing a newly developed wavelet-based index of storm activity (WISA) to the Dst index. The results show the wavelet analysis has its unique capability for separating the geomagnetic effects caused by different currents in magnetosphere and ionosphere. With its fully automatic procedure, high flexibility on data stretch, convenience of using data from a varying number of stations, high temporal resolution, and high tolerance for missing data from individual stations, the wavelet method is a perfectly suitable tool to study the time varying data such as geomagnetic data, because the wavelet analysis technique has the ability to present information in temporal and frequency domain at the same time. Such ability can be used to separate time varying signal into time series with different frequency variations. Applying the wavelet analysis to geomagnetic data can separate the geomagnetic effects connected to different currents in terms of different frequencies of their variations.

Second, after the geomagnetic field disturbances connected to the ring current variations are extracted from the total geomagnetic field by applying the wavelet analysis, visual comparison study, wavelet cross spectrum analysis, and magnitude comparison study are performed to investigate the characteristics of symmetric and asymmetric components on various time scales for both quiet and storm periods. Our results show during quiet periods, the magnetic effect of the symmetric ring current is comparable to that of the asymmetric (or local-time dependent) one and the slow time-varying components of the ring current are largely globally symmetric. During storm periods, the magnetic disturbances associated with both the symmetric and asymmetric parts of the ring currents increase significantly, but the increase of the symmetric ring current is much larger than that of the asymmetric current and it becomes dominant. This result is based on the statistical study of multiple-day timescale variations. For shorter timescales, such as the main phase of storms, the asymmetric component could be stronger than the symmetric component. Our results also indicate there are substantial residues of the magnetic effects of local-time-dependent currents left in the Dst index, and this further proves the Dst is not an ideal index for the description of the symmetric ring current.

Third, the variability of the symmetric ring current is studied by using geomagnetic data that are connected to the global symmetric ring current and reconstructed by the wavelet analysis for both storm and quiet periods. The complicated variations of the symmetric ring current are categorized into four simplified configurations including the radius variations, the intensity variations, the shift variations, and the tilt variations. Specifically, the radius variations of the symmetric ring current are studied by applying the wavelet analysis and electrodynamics schemes to the multiple components of ground-based geomagnetic data from multiple locations. The results show during quiet periods, the symmetric ring current normally stays at the radius of about 6 Re from the Earth and during storm periods, the symmetric ring current starts to move towards the Earth during the main phase, and moves away from the Earth during the recovery phase. The range of the radius variations is from 3 to 6 Re, depending on the magnitude of the geomagnetic disturbances. For a

strong geomagnetic storm, the symmetric ring current can move to as close as 3 Re. There is a time delay between the minimum of the storm main phase and the radius minimum of the symmetric ring current. The reasonable explanation is during the main phase of the geomagnetic storm, the asymmetric ring current is the most enhanced part, whereas the calculation in this research is focused on the symmetric ring current part. The symmetric ring current starts to become dominant after the main phase peak, and during the recovery periods, the symmetric ring current and the Dst index almost vary in phase. The results agree with the study of the ring current variations done by using satellite in-situ measurements. A mathematical scheme for deriving the ring current variations in both radius and intensity is discussed at the end. It can be a follow-on work to this dissertation.

The techniques developed in this dissertation research can be very useful for real-time monitoring of the dynamical variations of magnetic storm activities and the spatial and temporal variations of the ring currents. The scientific results of this research would shed light on our physical understanding of the dynamics of the ring current as well as the geomagnetic storm processes. Quantitative information on the spatial and temporal variability of the ring currents is crucial and invaluable for the national space weather program, and the techniques developed can be potentially used as a space weather monitoring tool for satellite controls, power grids, communication systems, oil pipelines, and other high-tech systems that are vulnerable to the negative impacts of disruptive geomagnetic events.

REFERENCES

[1] C. T. Russell and J. G. Luhmann, *Encyclopedia of Planetary Sciences.* London: Springer, 1997.

[2] T. Iijima and T. Potemra, "The amplitude distribution of field-aligned currents at northern high latitudes observed by triad," *J. Geophys. Res.*, vol. 81, no. 13, pp. 2165–2174, 1976.

[3] W. Gonzalez, J. Joselyn, Y. Kamide, H. Kroehl, G. Rostoker, B. Tsurutani, and V. Vasyliunas, "What is a geomagnetic storm?" *J. Geophys. Res.*, vol. 99, pp. 5771–5792, 1994.

[4] W. Kertz, "Ein neues mass fur die feldstarke des erdmagnetischen aquatorialen ringstroms, abh. akad. wiss. gottingen," *Math. Phys.*, vol. 2, p. 83, 1958.

[5] W. Kertz, "Ring current variations during the IGY," *Ann. Int. Geophys. Year*, pp. 35–49, 1964.

[6] M. Sugiura, "Hourly values of equatorial dst for the igy," *Annals of International Geophysical Year*, vol. 35, pp. 9–45, 1964.

[7] M. Sugiura and S. Hendricks, "Provisional hourly values of equatorial dst for 1961, 1962 and 1963," *NASA Tech. note*, vol. D-4047, 1967.

[8] M. Sugiura, "Resolution 2," *IAGA Bulletin 27*, p. 123, 1969.

[9] S. Akasofu, "The ring current, geomagnetic disturbance and the Van Allen radiation belts," *J. Geophys. Res.*, vol. 66, p. 1321, 1961.

[10] Y. Kamide, W. Baumjohann, I. A. Daglis, W. D. Gonzalez, M. Grande, and J. A. Joselyn, "Current understanding of magnetic storms: Storm-substorm relationships," *J. Geophys. Res.*, vol. 103, pp. 17,705–17,728, 1998.

[11] R. G. Rastogi, "Signatures of storm sudden commencements in geomagnetic h, y and z fields at Indian observatories during 1958-1992," *Ann. Geophys.*, vol. 17, pp. 1426–1438, 1999.

[12] I. A. Daglis, J. U. Kozyra, Y. Kamide, D. Vassiliadis, A. S. Sharma, M. W. Liemohn, W. D. Gonzalez, B. T. Tsurutani, and G. Lu, "Intense space storms: Critical issues and open disputes," *J. Geophys. Res.*, vol. 108, p. 1208, 2003.

[13] F. N. Okeke and Y. Hamano, "Daily variations of geomagnetic h d and z-field at equatorial latitudes," *Earth, Planets and Space*, vol. 52, pp. 237–243, 2000.

[14] K. J. Remick and J. J. Love, "Statistical modeling of storm-level kp occurrences," *Geosphys. Res. Lett.*, vol. 33, p. L16102, 2006.

[15] I. A. Daglis and J. U. Kozyra, "Outstanding issues of ring current dynamics," *J. Atmos. Solar-Terr. Phys.*, vol. 64, pp. 253–264, 2002.

[16] C. T. Russell and D. E. Huddleston, "Predicting the strength of the ring current," *Adv. in Space Res*, vol. 20, no. 3, pp. 327–334, 1997.

[17] N. Y. Ganushkina, T. I. Pulkkinen, M. V. Kubyshkina, H. J. Singer, and C. T. Russell, "Modeling the ring current magnetic field during storms," *J. Geophys. Res.*, vol. 107, p. 1092, 2002.

[18] F. Soraas, K. Aarsnes, K. Oksavik, and D. S. Evans, "Ring current intensity estimated from low altitude proton observations," *J. Geophys. Res.*, vol. 107, p. 1149, 2002.

[19] W. D. Gonzalez, A. D. Lagoa, A. L. C. de Gonzaleza, L. E. A. Vieiraa, and B. T. Tsurutanib, "Prediction of peak-dst from halo cme/magnetic cloud-speed observations," *J. Atmos. and Solar-Terr. Phys.*, vol. 66, pp. 161–165, 2004.

[20] J. M. Weygand and R. L. McPherron, "Dependence of ring current asymmetry on storm phase," *J. Geophys. Res.*, vol. 111, p. A11221, 2006.

[21] G. Le, C. T. Russell, and K. Takahashi, "Morphology of the ring current derived from in-situ magnetic field measurements," *Ann. Geophys.*, vol. 22, pp. 1267–1295, 2004.

[22] D. C. Hamilton, G. Gloeckler, F. M. Ipavich, B. W. W. Studemann, and G. Kremser, "Ring current development during the great geomagnetic storm of February 1986," *J. Geophys. Res.*, vol. 93, no. A12, pp. 14,343–14,355, 1988.

[23] W. H. Campbell, "Failure of dst index fields to represent a ring current," *Space Weather*, vol. 2, p. S08002, 2004.

[24] A. Karinen and K. Mursula, "A new reconstruction of the dst index for 1932-2002," *Ann. Geophys.*, vol. 23, no. 2, pp. 475–485, 2005.

[25] A. Karinen and K. Mursula, "Correcting the dst index: Consequences for absolute level and correlations," *J. Geophys. Res.*, vol. 111, p. A08207, 2006.

[26] J. A. Wanliss and K. M. Showalter, "High-resolution global storm index: Dst versus sym-h," *J. Geophys. Res.*, vol. 111, p. A02202, 2006.

[27] T. P. O'Brien and R. L. McPherron, "An empirical phase space analysis of ring current dynamics: Solar wind control of injection and decay," *J. Geophys. Res.*, vol. 105, no. A4, pp. 7707–7719, 2000.

[28] A. Jach, P. Kokoszka, J. Sojka, and L. Zhu, "Wavelet-based index of magnetic storm activity," *J. Geophys. Res.*, vol. 111, p. A09215, 2006.

[29] J. Rees, C. Wilford, R. Moffett, Z. Dent, and I. Mann, "Analysis of magnetometer data using wavelet transform," *Trans. R. Soc. Lond. A.*, vol. 361, pp. 133–137, 2003.

[30] H. L. Wei, S. A. Billings, and M. Balikhin, "Prediction of the dst index using multiresolution wavelet models," *J. Geophys. Res.*, vol. 109, p. A07212, 2004.

[31] A. Grinsted, J. C. Moore, and S. Jevrejeva, "Application of the cross wavelet transform and wavelet coherence to geophysical time series," *Nonlinear Processes Geophys.*, vol. 11, pp. 561– 566, 2004.

[32] S. R. Nayar, V. N. Radhika, and P. T. Seena, "Investigation of substorms during geomagnetic storms using wavelet techniques," *Paper presented at ILWS Workshop, Goa, India,*, pp. 19–24, 2006.

[33] D. Heslop, "A wavelet investigation of possible orbital influences on past geomagnetic field intensity," *Geochem. Geophys. Geosyst.*, vol. 8, p. Q03003, 2007.

[34] Z. Xu, L. Zhu, J. J. Sojka, P. Kokoszka, and A. Jach, "An assessment study of the wavelet-based index of magnetic storm activity (WISA) and its comparison to the dst," *J. Geophys. Res.*, vol. 70, pp. 1579–1588, 2008.

[35] Z. Xu, L. Zhu, J. J. Sojka, and P. Kokoszka, "Wavelet cross-spectrum analysis of the ring current using magnetic records from multiple low-latitude stations," *J. Geophys. Res.*, vol. 114, p. A05309, 2009.

[36] Z. Xu, L. Zhu, J. J. Sojka, and P. Kokoszka, "Study of geomagnetic disturbances and ring current variability during strom and quiet times using wavelet analysis and ground-based magnetic data from multiple stations," *the American Geophysical Union Fall Meeting in San Francisco*, 2010.

[37] W.-Y. Xu and Y. Kamide, "Decomposition of daily geomagnetic variations by using method of natural orthogonal component," *J. Geophys. Res.*, vol. 109, p. A05218, 2004.

[38] W. H. Campbell, "Geomagnetic storms, the dst ring-current myth,and lognormal distributions," *J. Atmos. Terr. Phys.*, vol. 58, pp. 1171–1187, 1996.

[39] O. J. Mendes, A. Mendes da Costa, and F. C. P. Bertoni, "Effects of the number of stations and time resolution on dst derivation," *J. Atoms. Sol. Terr. Phys.*, vol. 68, pp. 2127–2137, 2006.

[40] W. H. Campbell, "Comment on current understanding of magnetic storms: Storm-substorm relationships by Y. Kamide et al." *J. Geophys. Res.*, vol. 104, pp. 7049–7049, 1999.

[41] T. Iyemori, A. T., T. Kamei, and M. Takeda, "Mid-latitude geomagnetic indices asy and sym (provisional)," *Kyoto Univ., Kyoto, I-X.*, vol. 6, 1996.

[42] C. Stoermer, "Sur la situation de la zone de frequence maximum des aurores boreales dapres la theorie corpusculaire," *C. R. Acad. Sci.*, vol. 151, pp. 736–739, 1910.

[43] C. Stoermer, "Sur les trajectories des corpuscules electrises dans l'espace sous l'actions des magnetisme terrestre avec application aux auarores boreales, seconde memoir," *Arch Sci. Phys. Nat.*, vol. 4, no. 32, pp. 117–123, 190–219, 277–314, 415–436, 505–509, 1911.

[44] C. Stoermer, "Sur les trajectories des corpuscules electrises dans l'espace sous l'actions des magnetisme terrestre avec application aux auarores boreales, seconde mernoire (continued)," *Arch. Sci. Phys. Nat.*, vol. 4, no. 33, pp. 51–69, 113–150, 1912.

[45] A. Schmidt, "Das erdmagnetische aussenfeld," *Z. Geophys.*, vol. 1, pp. 3–13, 1924.

[46] S. Chapman and V. C. A. Ferraro, "A new theory of magnetic storms, i, the initial phase," *J. Geophys. Res.*, vol. 36, pp. 77–97,171–186, 1931.

[47] S. Chapman and V. C. A. Ferraro, "A new theory of magnetic storms, i, the initial phase (continued)," *J. Geophys. Res.*, vol. 37, pp. 147–156,421–429, 1932.

[48] S. Chapman and V. C. A. Ferraro, "A new theory of magnetic storms, ii, the main phase," *J. Geophys. Res.*, vol. 38, pp. 79–96, 1933.

[49] H. Alfven, "The theory of magnetic storms and auroras," *Nature*, vol. 167, p. 984, 1951.

[50] E. J. Smith, "Theoretical and experimental aspects of ring currents," *Space Science*, pp. 316–373, 1963.

[51] S. F. Singer, "A new model of magnetic storms and aurorae," *Eos (Trans. AGU*, vol. 38, pp. 175–190, 1957.

[52] A. Dessler and E. N. Parker, "Hydromagnetic theory of geomagnetic storms," *J. Geophys. Res.*, vol. 64, pp. 2239–2252, 1959.

[53] S. Akasofu, "In memoriam Sydney Chapman," *Space Sci. Rev.*, vol. 11, pp. 599–606, 1970.

[54] R. K. Burton, R. L. McPherron, and C. T. Russell, "An empirical relationship between interplanetary conditions and dst," *J. Geophys. Res.*, vol. 80, no. 31, pp. 4204–4214, 1975.

[55] L. R. Lyons and M. Schulz, "Access of energetic particles to storm time ring current through enhanced radial diffusion," *J. Geophys. Res.*, vol. 94, p. 5491, 1989.

[56] I. I. Alexeev, E. S. Belenkaya, V. V. Kalegaev, Y. I. Feldstei, and A. Grafe, "Magnetic storms and magnetotail currents," *J. Geophys. Res.*, vol. 101, no. A4, pp. 7737–7747, 1996.

[57] D. Vassiliadis, A. J. Klimas, and D. N. Baker, "Models of dst geomagnetic activity and of its coupling to solar wind parameters," *Physics and Chemistry of the Earth*, vol. 24, pp. 107–112, 1999.

[58] F. Soraas and M. Sorbo, "Ring current behaviour inferred from ground magnetic and space observations," *American Geophysical Union, Spring Meeting 2007*, pp. SM31A–03, 2007.

[59] Y. Wu, W. Xu, G. Chen, B. Chen, and X. Liu, "Ground magnetic characteristics of the storm-time ring current asymmetry," *Sci China Ser D-Earth Sci*, vol. 51, no. 5, pp. 686–693, 2008.

[60] L. Zhu, J. J. Sojka, R. W. Schunk, Z. Xu, and P. Kokoszka, "Study of the ring current variability with the use of ground-based magnetometer measurements and new statistical technique: Preliminary results," *American Geophysical Union, Fall Meeting 2009*, pp. SM11A–1538, 2009.

VITA

Zhonghua Xu

EDUCATION:

Ph.D., Physics (2005-2011), Department of Physics, Utah State University, Logan, Utah, USA.

B.S., Geophysics (1995-1999), Department of Geophysics, Beijing University, Beijing, China.

PROFESSIONAL EXPERIENCE:

Graduate Research Assistant (2005-2011), Center for Atmospheric and Space Sciences, Utah State University.

Graduate Teaching Assistant (2009-2011), Department of Physics, Utah State University.

Research Assistant (1999-2005), Department of Upper Atmospheric Physics, Polar Research Institute of China, Shanghai, China.

Antarctic Expedition (1999-2001), Upper Atmospheric Physics Lab, Chinese Antarctic Zhongshan Station, 16th Chinese Antarctic Expedition Team.

PUBLICATIONS:

Xu, Z., L. Zhu, J. Sojka, and P. Kokoszka (2009), Wavelet cross-spectrum analysis of the ring current using magnetic records from multiple low-latitude stations, J. Geophys. Res., 114, A05309, doi:10.1029/2009JA014076.

Xu, Z., L. Zhu, J. Sojka, P. Kokoszka, and A. Jach (2008), An assessment study of the wavelet-based index of magnetic storm activity(WISA) and its comparison to the Dst, Journal of Atmospheric and Solar-Terrestrial Physics Volume 70, Issues 11-12, August 2008, Pages 1579-1588 doi:10.1016/j.jastp.2008.05.007.

Xu Zhong-Hua, LIU Rui-Yuan, LIU Shun-Lin, ZHANG Bei-Chen, HU Hong-Qiao, and QI Xin, Variations of the ionospheric F2 layer critical frequency at Zhongshan Station, Antarctica, CHINESE JOURNAL OF GEOPHYSICS, 2006 Vol.49 No.1 P.1-8.

R. Liu, Z. Xu, J. Wu, S. Liu, B. Zhang, and G. Wang (2005): Preliminary studies on ionospheric forecasting in China and its surrounding area, J. Atmos. Sol. Terr. Phys., 67(12), 1129-1136.

Lie Zhu, Zhonghua Xu, Jan J. Sojka, Robert W. Schunk, Pior Kokoszka, and Agnieszka Jach, Are the Dst Stations Sufficient for Describing Storm-Time Enhancements, presented at the International Union of Geodesy and Geophysics (IUGG) XXIV General Assembly in Perugia, Italy, 2-13 July 2007.

Liu Ruiyuan, Liu Shunlin, Xu Zhonghua, Wu Jian, Wang Xianyi, Zhang Beichun, and H. Hu, The Application of Autocorrelation Method In Short-term Forecasting of the Ionosphere in China Region, Chinese Science Bulletin, Vol 50, pages 2781-2785, December 2005, DOI: CNKI:SUN:KXTB.0.2005-24-016.